深圳综合粒子设施研究院
Institute of Advanced Science Facilities, Shenzhen

THE HONG KONG POLYTECHNIC UNIVERSITY
香港理工大學

For Croucher 4th Generation Synchrotron Radiation Summer School

Hard X-Ray Nanoscale Microscopy Nanoprobe and TXM

Lei Li（李雷），Yitao CUI（崔艺涛）*

@PolyU 2024-06-18

Content

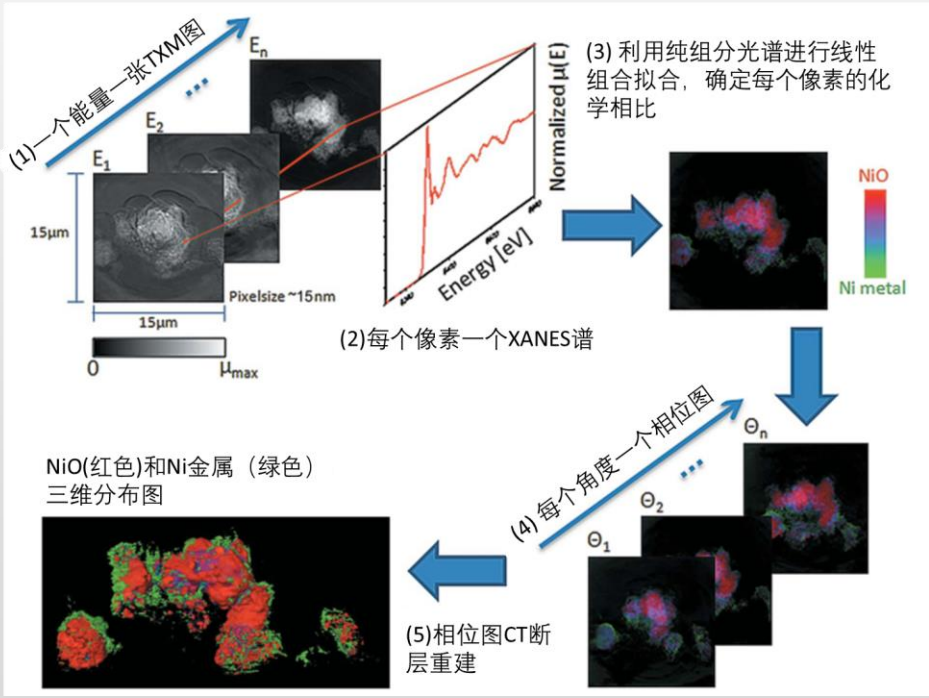


- Hard X-ray Nanoprobe
- Full-field Transmission X-ray Microscopes，TXM

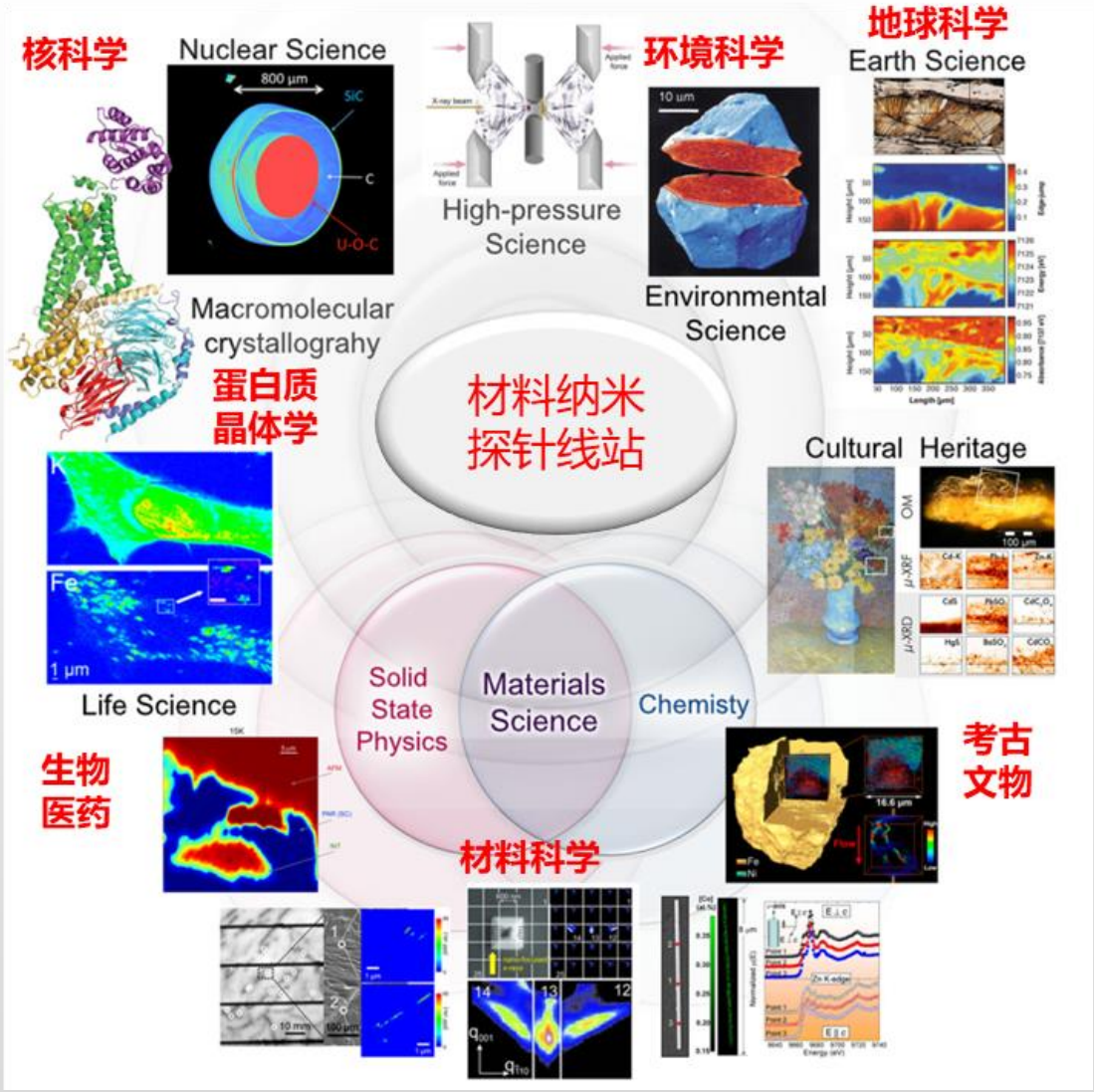
x-ray nanoprobe

深圳综合粒子设施研究院
Institute of Advanced Science Facilities, Shenzhen

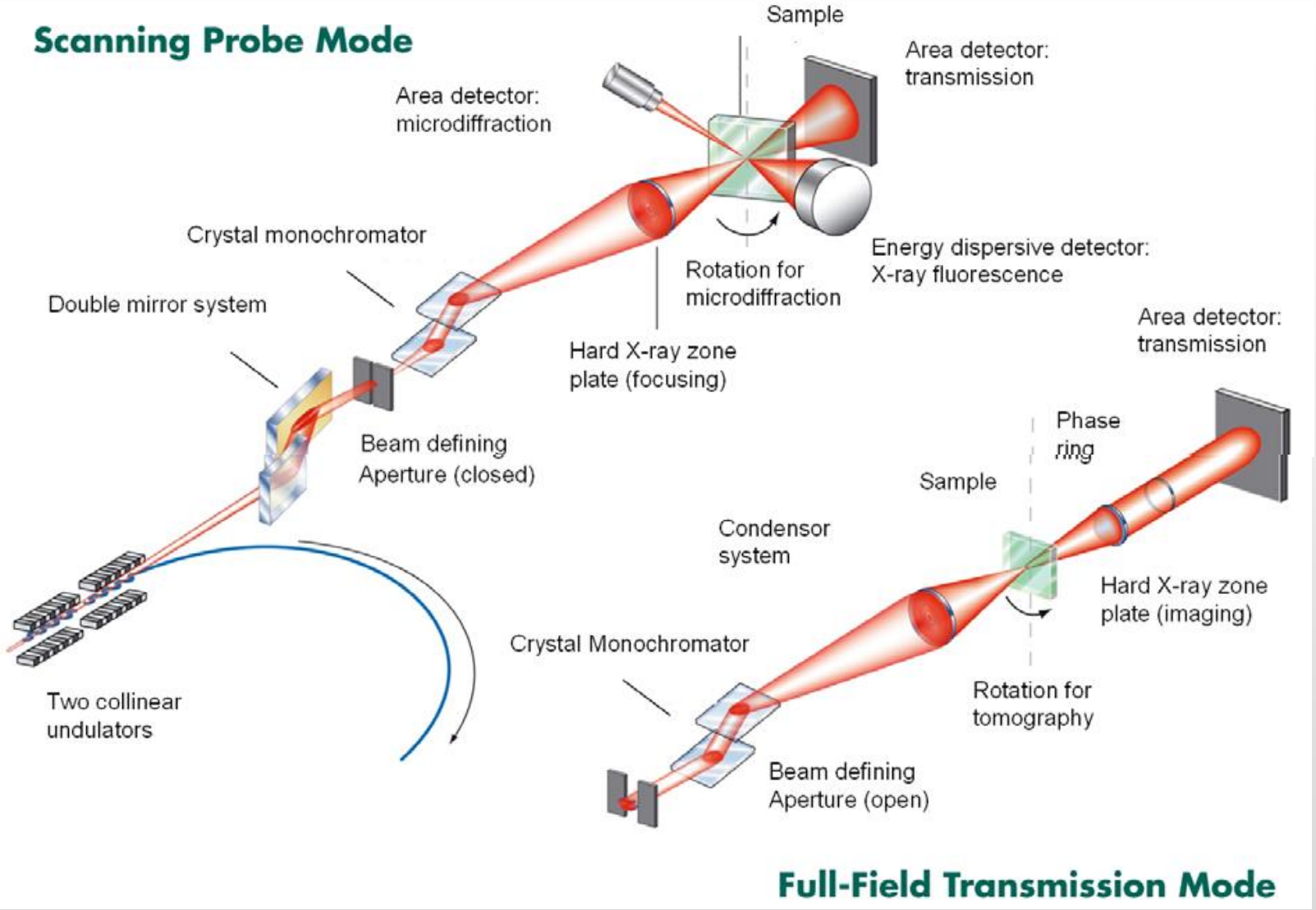
- **Usually, we need nano-resolution images together with element distribution as well as valence in 3D space, the combination of multiple method both with spectroscopy and nanoscale space resolution technique.**



methods
Nano-XRD
Nano-XRF
Nano-XAS
Nano-CT
Ptychography
TXM
XPCS
CXDI
Multiple method



Two common x-ray microscopes



- 10-20 nm spatial resolution
- Least radiation dose
- Best spectral resolution
- Requires spatially coherent radiation
- Minutes exposure time
- Flexible sample environment
- Photoemission, fluorescence imaging

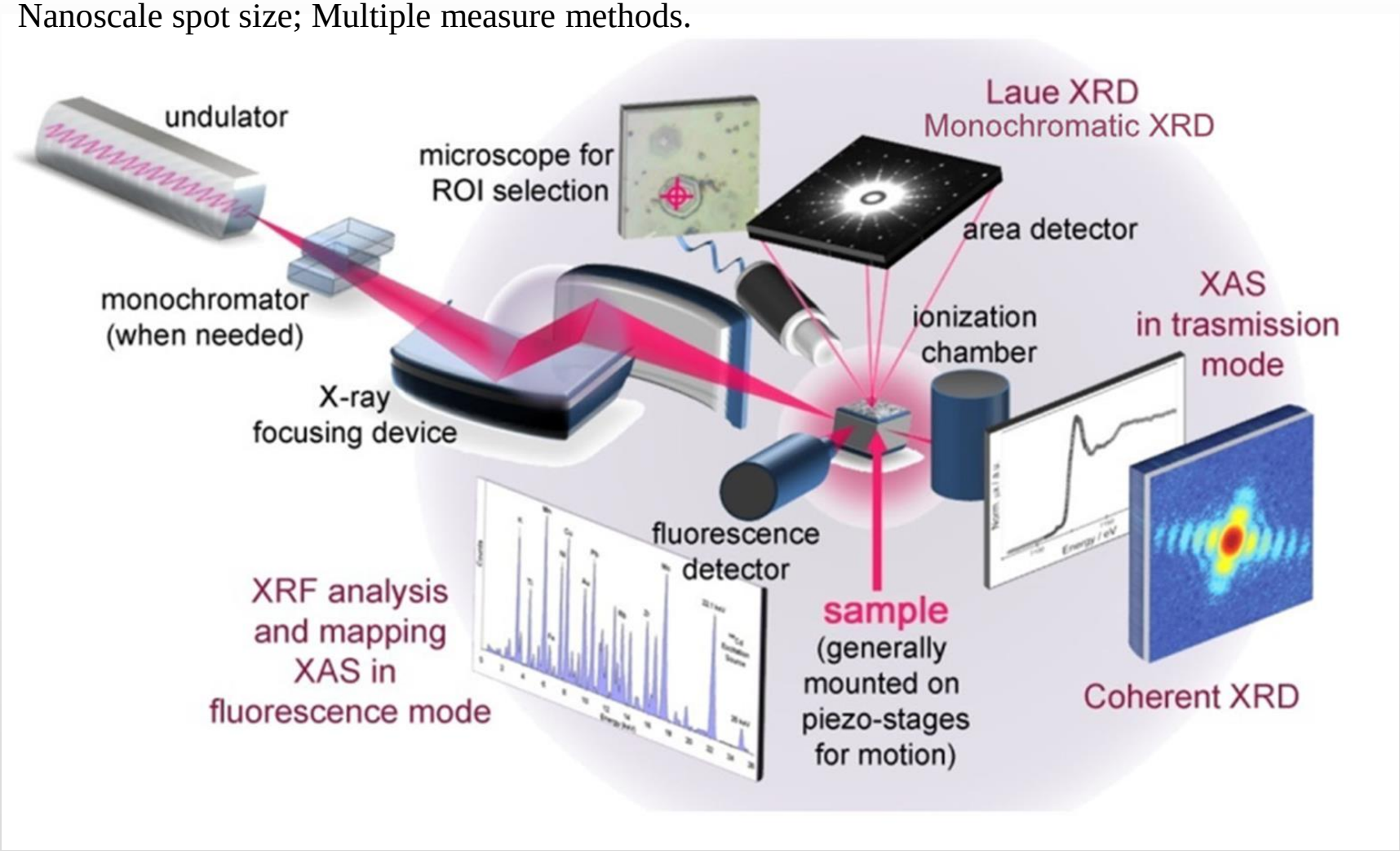
- 10-20 nm spatial resolution
- Modest spectral resolution
- Seconds exposure time
- Bending magnet radiation
- Higher radiation dose
- Flexible sample environment (wet, cryo, labeled magnetic fields, electric fields, cement, ...)

Hard X-ray Nanoprobe



Measure Methods

Nanoscale spot size; Multiple measure methods.



Mainly Methods:

- ✓ Nano-XRF
- ✓ Nano-XAFS
- ✓ Nano-XRD
- ✓ Ptychography
- ✓ Integrated
- ✓ …

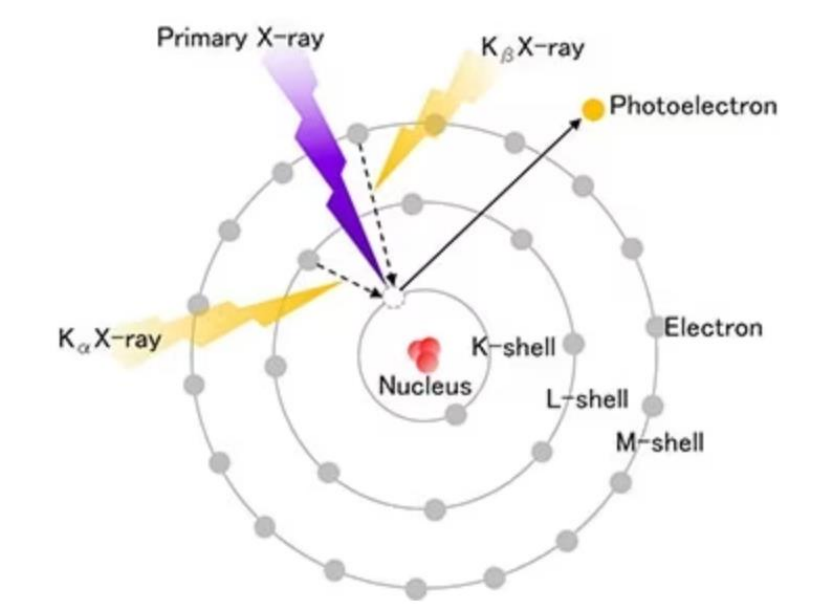
Rev. Mod. Phys. 90, 025007 (2018).

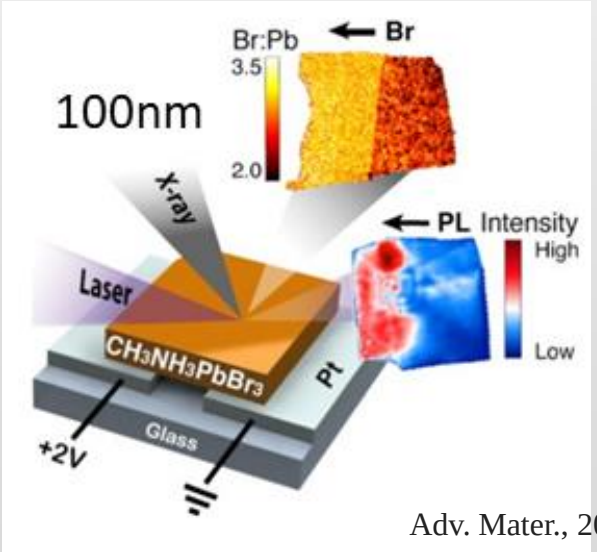
Nano-XRF

X-ray fluorescence (XRF) analysis is one of the best analytical techniques to perform nondestructive elemental analysis of solid or liquid samples for major and minor components. A sample is excited by bombarding with X-rays causing ejection of inner electrons with subsequent emission of the characteristic (fluorescence) X-rays of the sample. The energy of the fluorescence X-rays is a **characteristic** of an element, and their intensities are proportional to the number of excited atoms and thus can be used for qualitative and quantitative analysis of the sample .

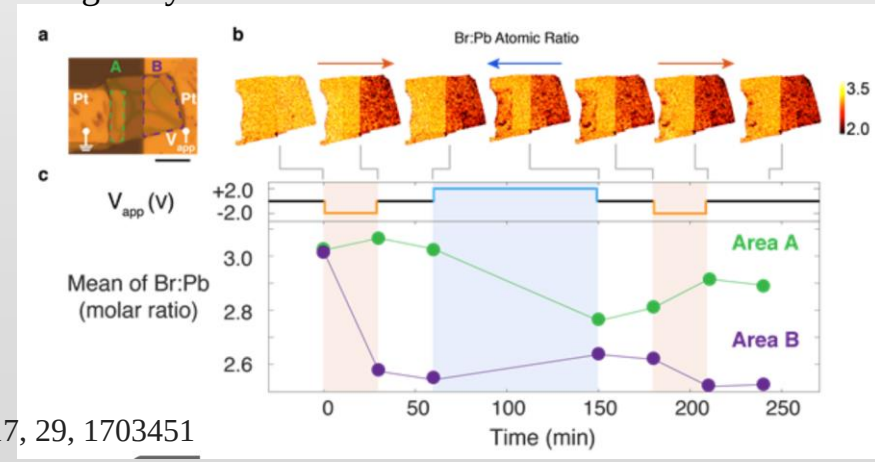
Advantages: ①non-destructive; ②multi-element simultaneous analysis; ③ high sensitivity; ④low detection limit (ppb); ⑤high spatial resolution (nm).

Principle





Changes in elemental distribution in a $H_3NH_3PbBr_3$ single crystal under bias



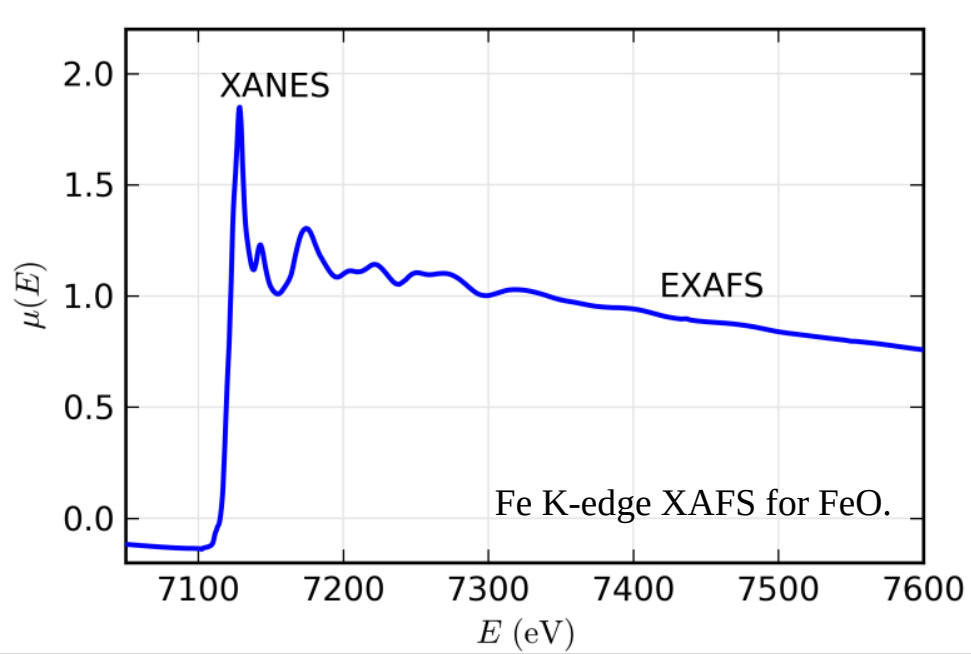
Adv. Mater., 2017, 29, 1703451

Nano-XAFS

深圳综合粒子设施研究院
Institute of Advanced Science Facilities, Shenzhen

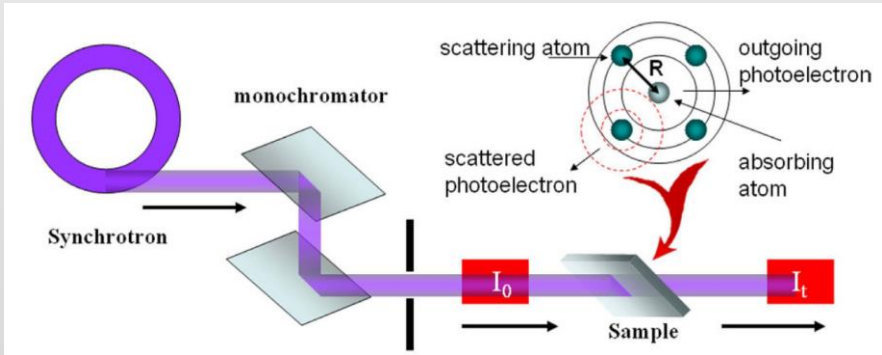
X-ray Absorption Spectroscopy (XAS) is the modulation of the X-ray absorption coefficient at energies at and above an X-ray absorption edge. Owing to its element specific and short-range nature, core-level XAS is widely used to elucidate the **local structural**, **vibrational**, and other physical properties of complex, aperiodic materials.

XAFS: X-ray Absorption Fine-Structure Spectroscopy (=XAS)
XANES: X-ray Absorption Near-Edge Spectroscopy
EXAFS: Extended X-ray Absorption Fine-Structure



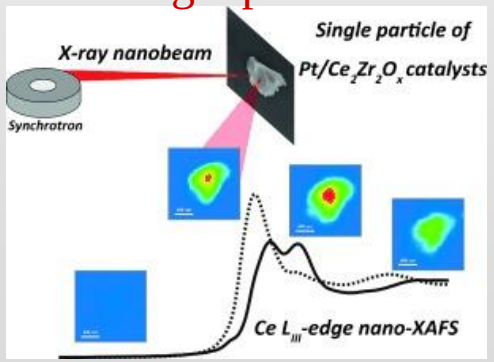
Main Characteristics: ①local atomic coordination; ②valence, oxidation state; ③applies to any element (Z > 2); ④minimal sample requirements; ⑤independent of crystal structure, isotope.

Bulk



Conventional XAFS

Single particle



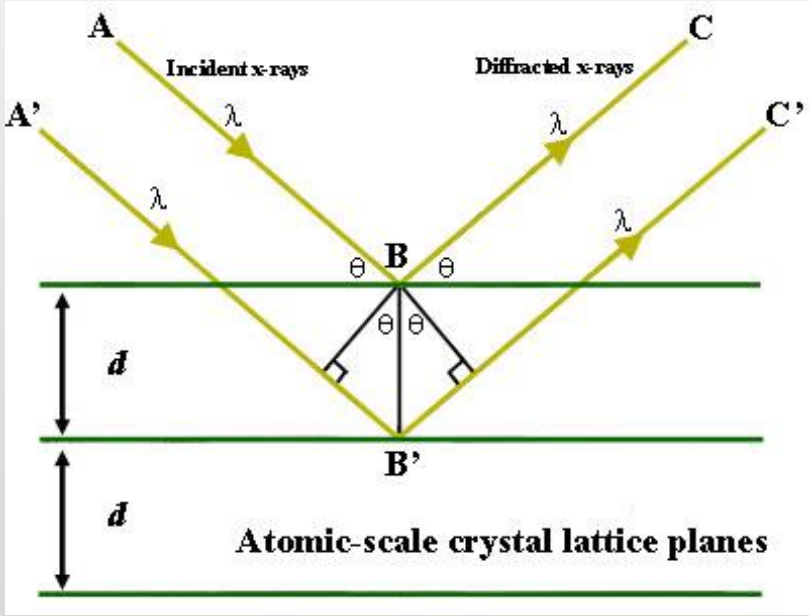
Nano-XAFS

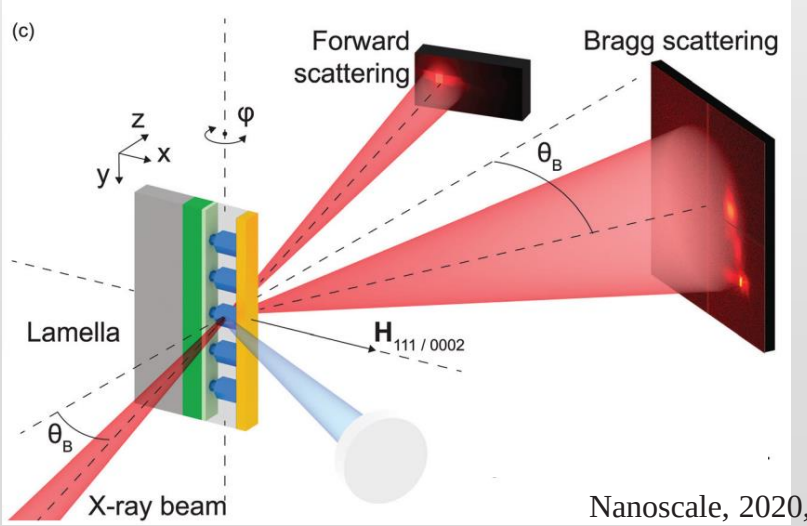
Nano-XRD

X-Ray diffraction (XRD) analysis is a common nondestructive technique that provides detailed information about the **crystallographic structure**, **chemical composition**, and physical properties of a material. Each phase of the material produces a unique diffraction pattern due to the material's specific chemistry and atomic arrangement.

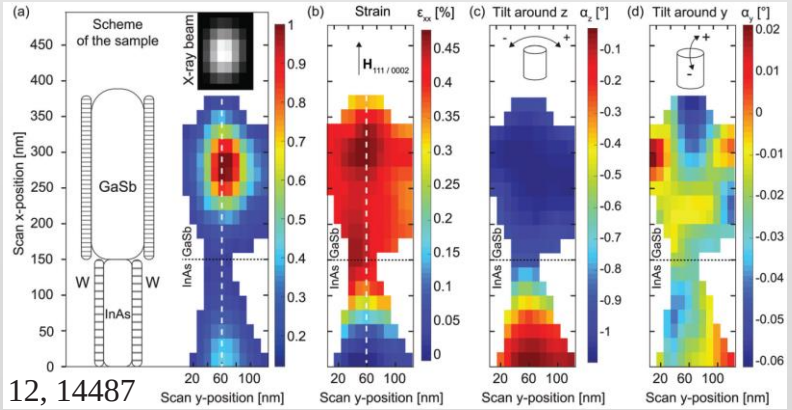
Key Features: ①Phase identification; ②Crystallite size estimation; ③Strain measurement; ④Texture analysis; ⑤Quantitative analysis.

Bragg's Law: $\sin\theta_{hkl} = n\lambda / 2d_{hkl}$





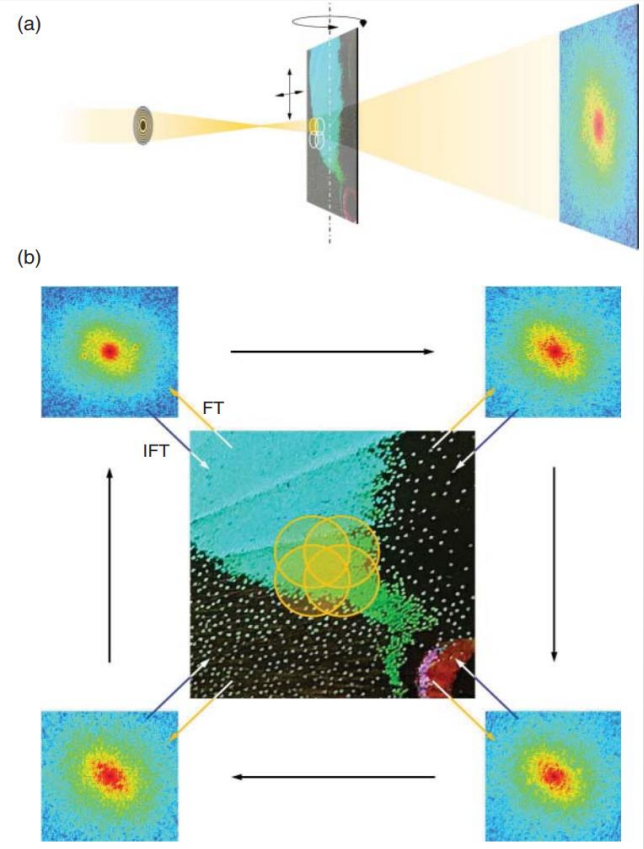
Diffraction mapping => Local strains and tilts

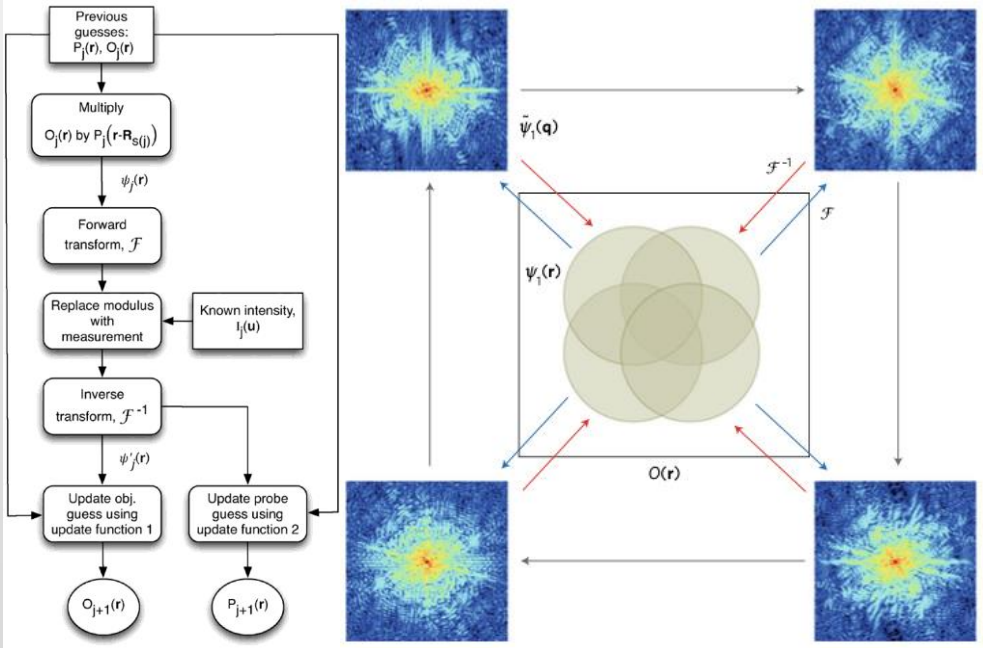


Nanoscale, 2020, 12, 14487

Ptychography

X-ray ptychographic microscopy combines the advantages of scanning X-ray microscopy with the coherent diffraction imaging. It is limited neither by the fabricational challenges associated with X-ray optics nor by the requirements of isolated specimen preparation, and offers in principle **wavelength-limited resolution**, as well as stable access and solution to the phase problem.

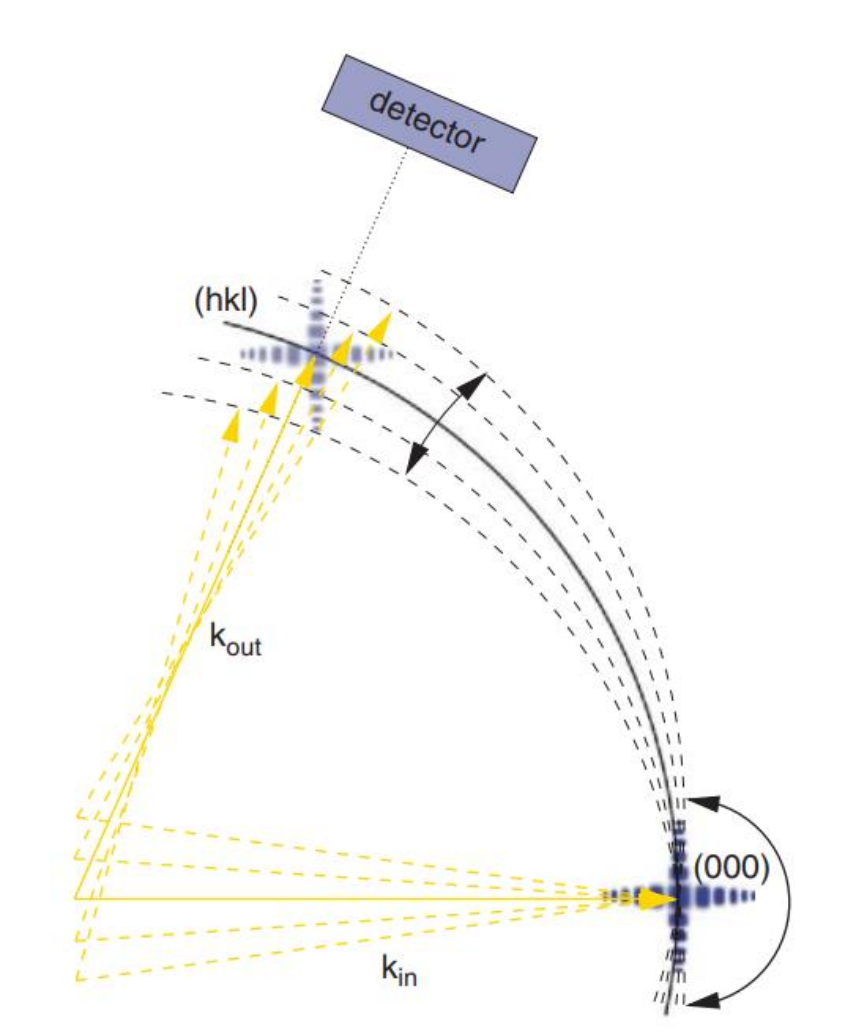




The sample area is scanned through multiple ptychographic scanning method, and then the amplitude and phase informations are reconstructed using relevant retrieval algorithm.

The reconstruction image finally shows structural details with a nanoscale resolution.

Bragg-Ptychography



Amorphous samples: Signals are usually collected in the forward scattering direction around the directly transmitted beam.

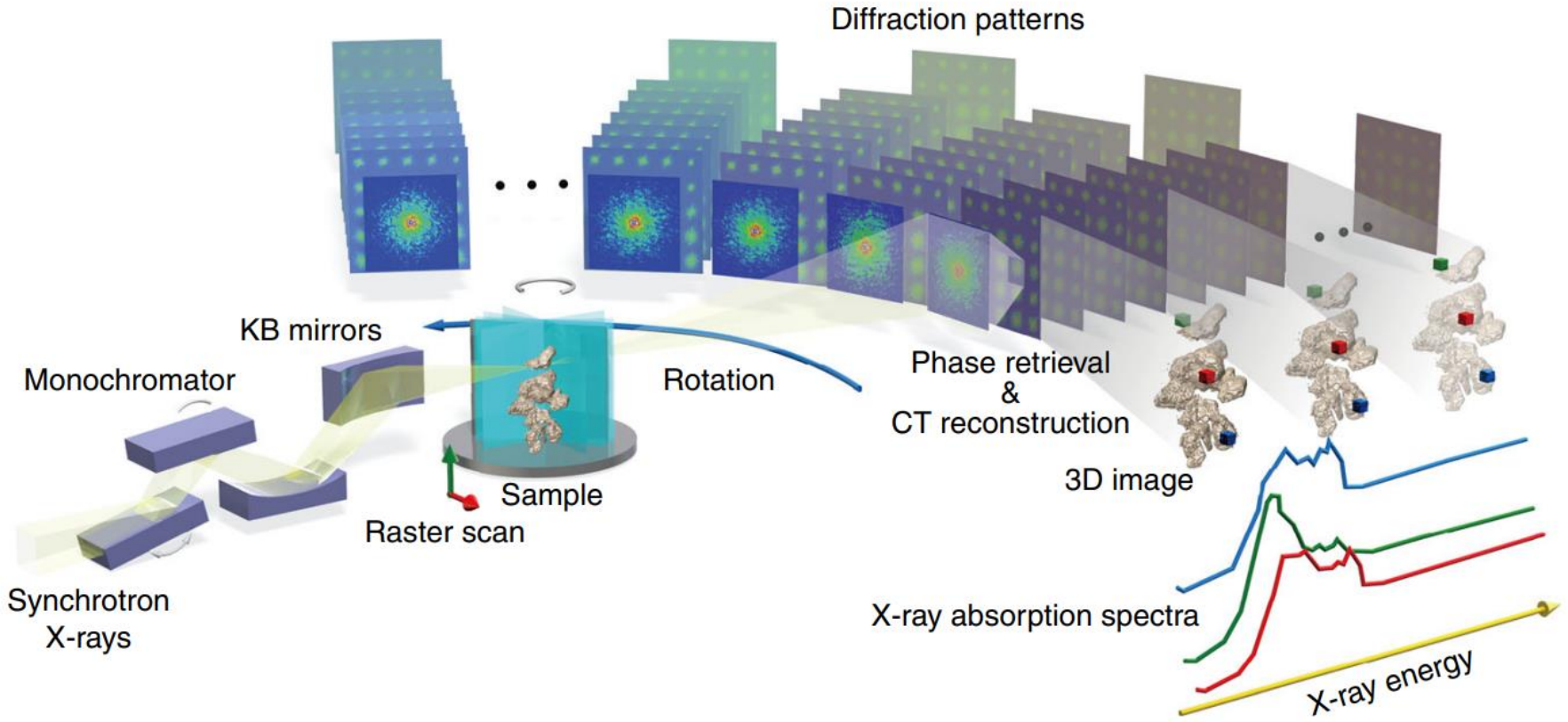
Crystallized samples: Signals can be collected at the Bragg point far away from the main optical axis, that is, characterized by Bragg-Ptychography.

Advantages of Bragg-Ptychography：

- Beamstop can be eliminated (which blocks part of the reconstructed feature) and the effect of diffuse scattering on the sample signal can be avoided;
- Sensitive to crystal defects and stress fields;
- The required of angle rotation is much smaller than for amorphous samples.

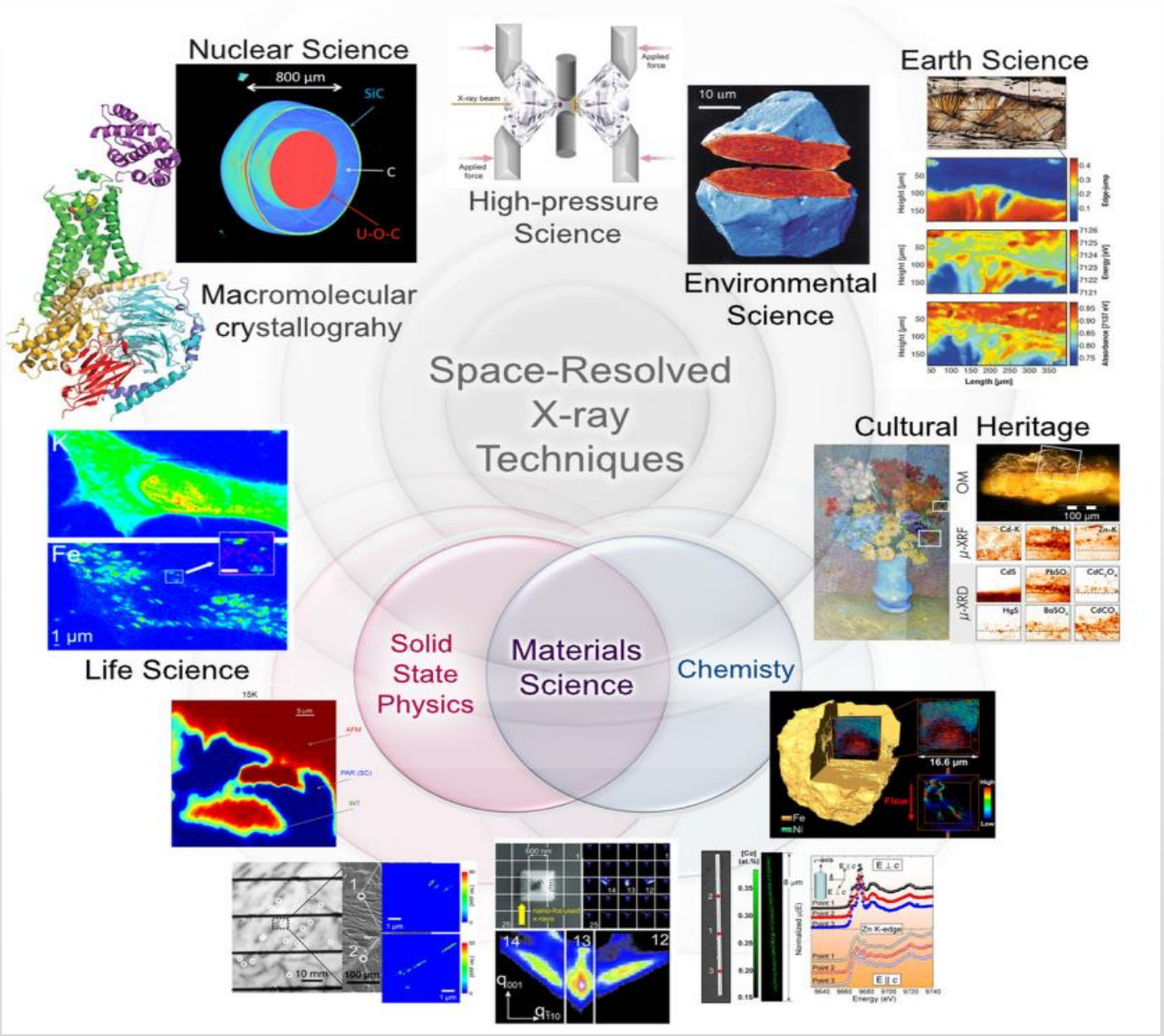
Integrated

In material characterization, it is usually necessary to complete multiple characterizations in morphology, phase, structure, composition, and valence state at the same time, so as to understand the physical, chemical and mechanical properties of materials.



Actual testing usually requires combining multiple measure methods.

Applications



Spatial Resolution → **Macro (mm)** → **Micro (μm)** → **Nano (nm)**

Nanoscale Characterization

Morphology, structure, elements, chemical state at nanometers



The “EYE” of Nanomaterials

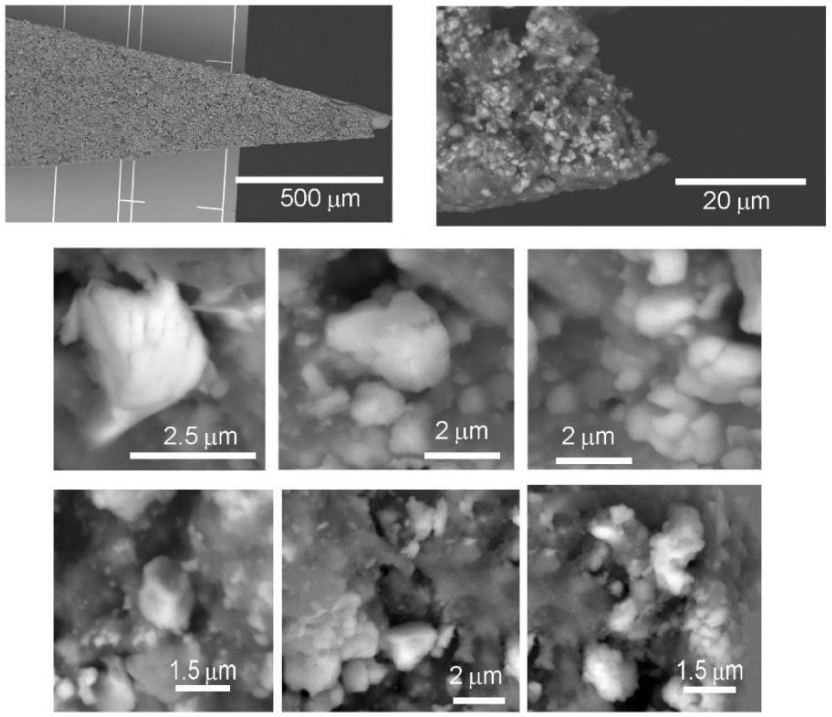
See the tiny space

Rev. Mod. Phys. 90, 025007 (2018).

Application: Lithium Ion Battery

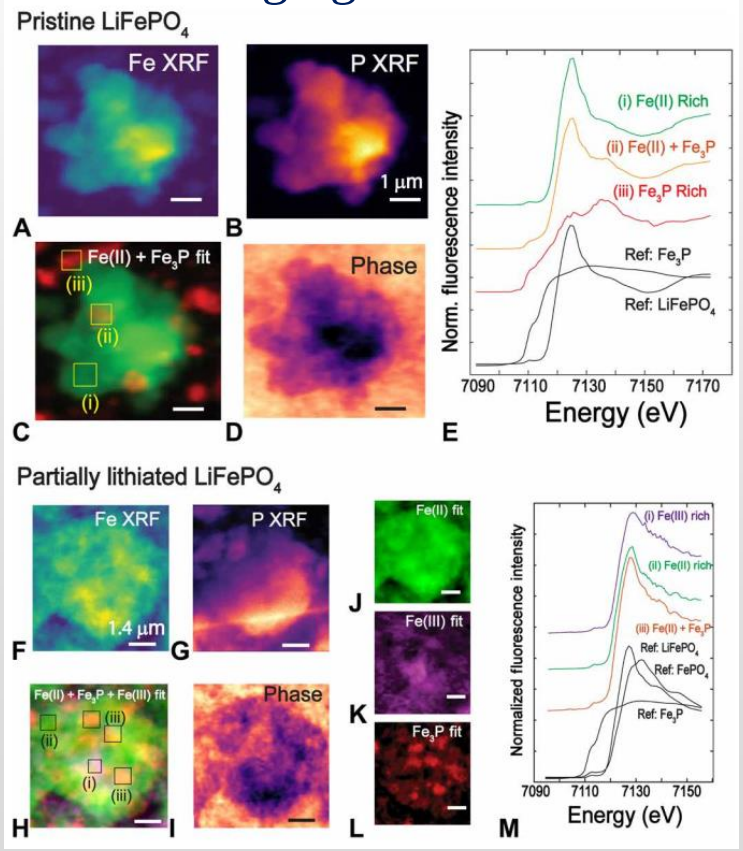
Nano-XANES was used to study the trace secondary phases in lithium iron phosphate (LFP) particles. Authors observed individual Fe-phosphide nanoparticles in pristine LFP, whereas partially (de)lithiated particles showed Fe-phosphide nanonetworks.

SEM images



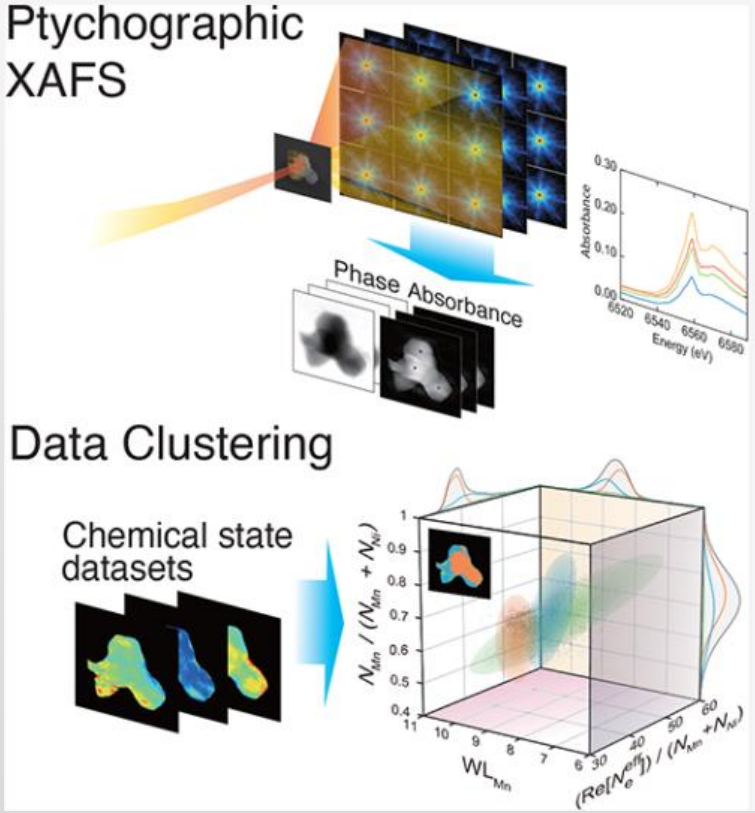
No morphology resembling to Fe-phosphide networks are observed on the particle surface.

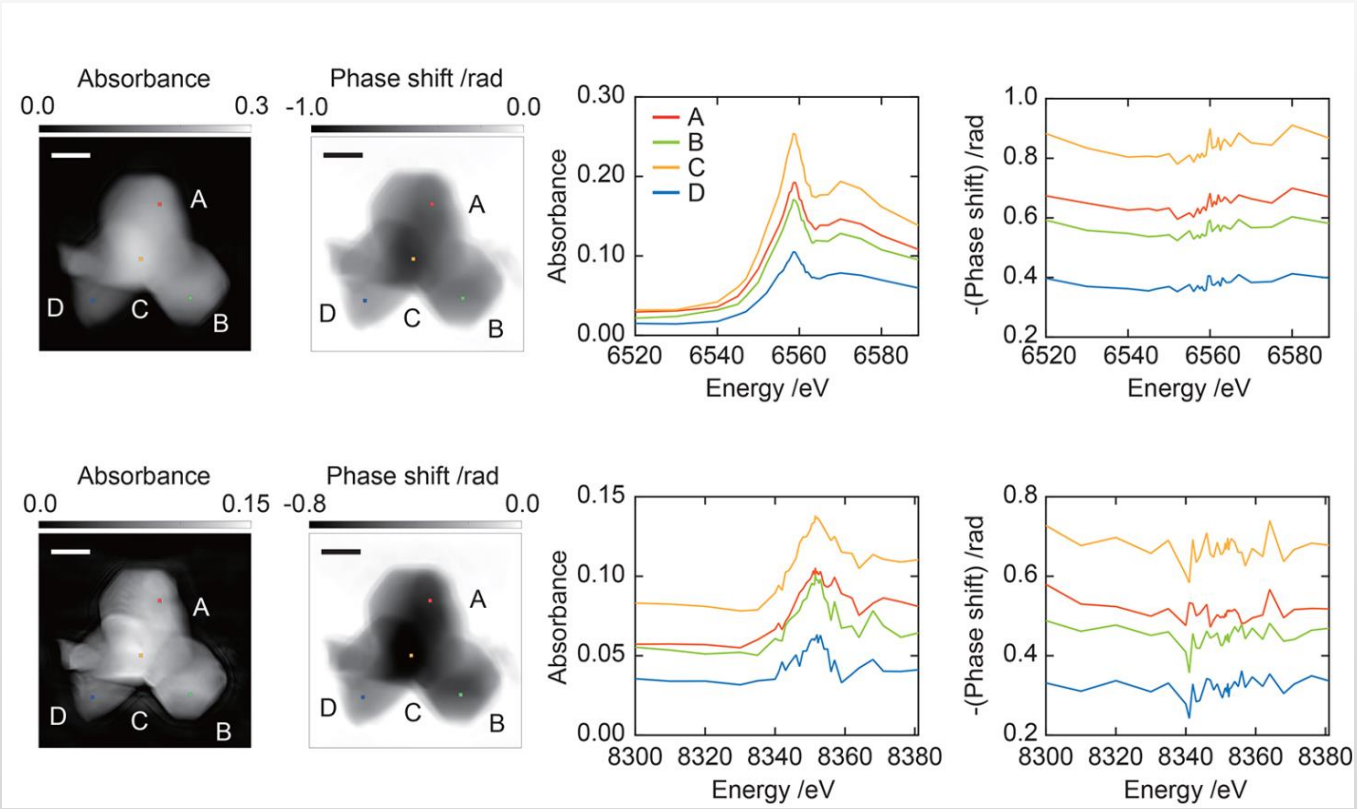
Chemical imaging with nano-XANES



Application: Lithium Ion Battery

Two-dimensional ptychographic XAFS was used to visualize the density and valence maps of manganese and nickel in as-prepared lithium nickel manganese oxides (LNMO) particles. The approach may increase the supply of information for nanoscale characterization and promote the design of suitable structural.

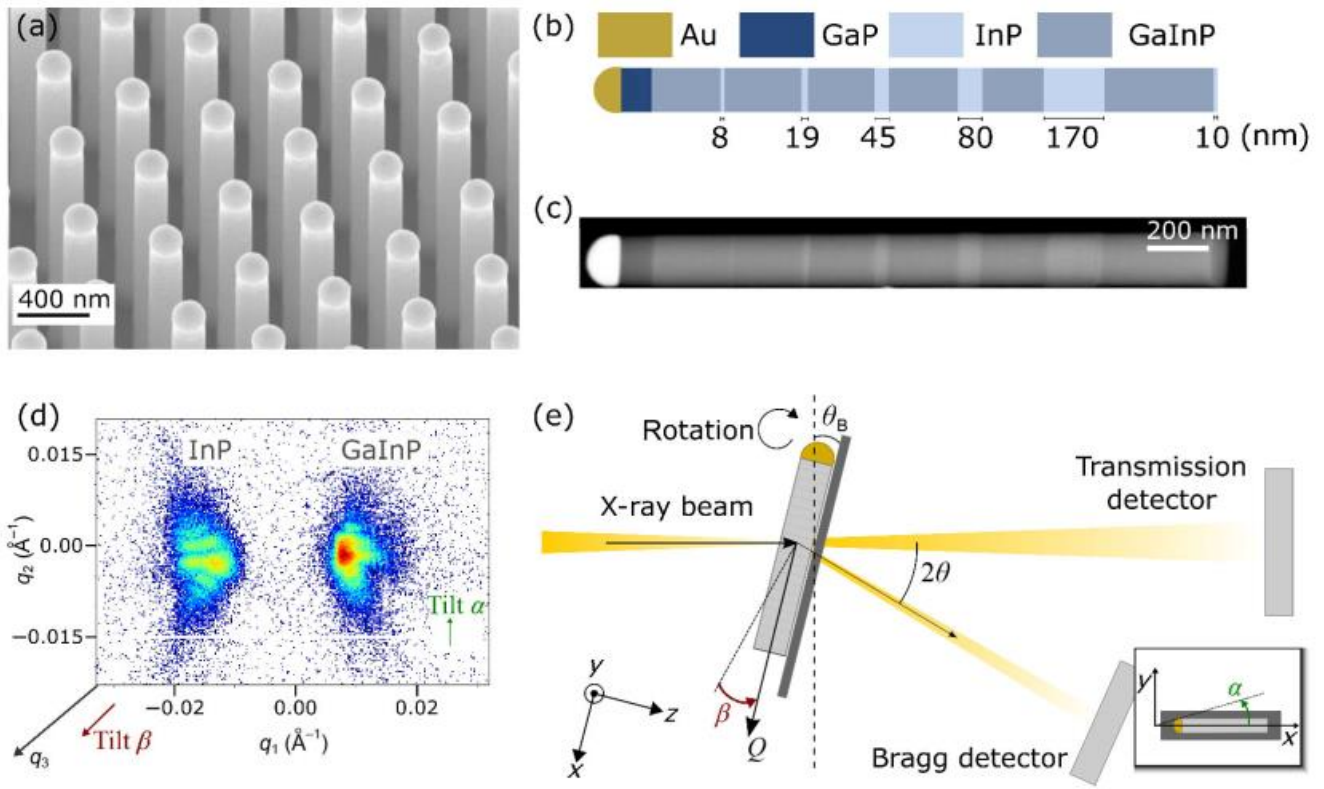


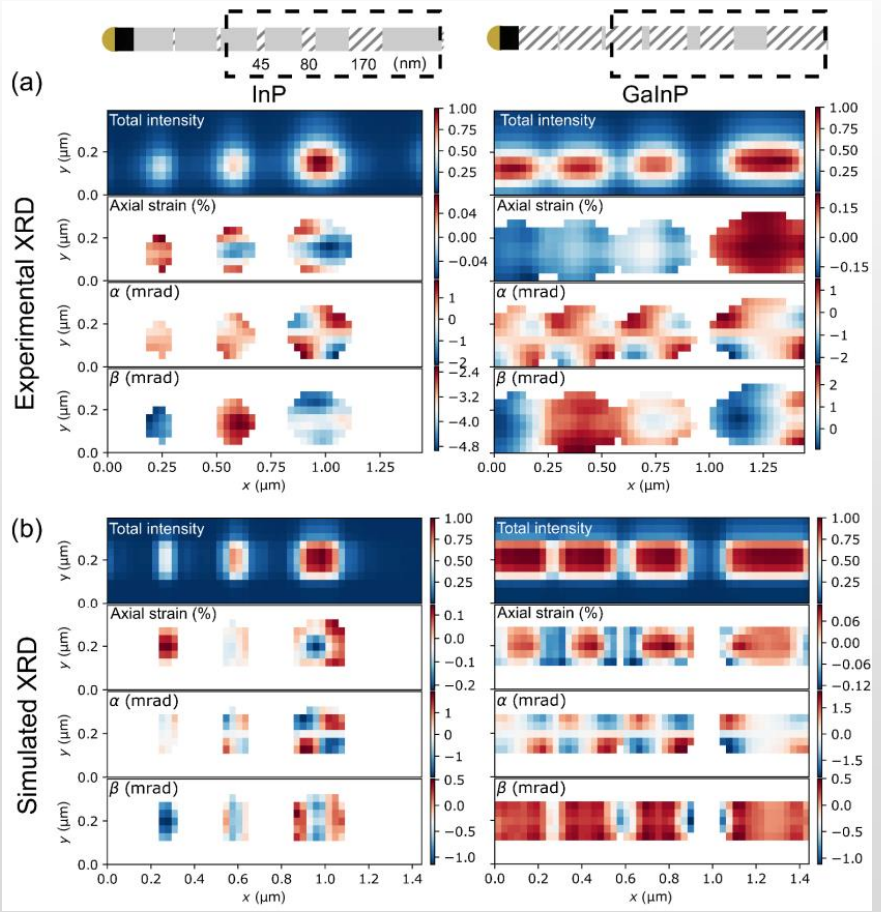


J. Phys. Chem. Lett. 2021, 12, 24, 5781–5788

Application: Nanoelectronics

Nano-XRD was used to obtain two-dimensional (2D) maps of the strain, with about 10^{-4} relative strain sensitivity, as well as the lattice tilt. These results demonstrate that nanofocused XRD has sufficient strain sensitivity and spatial resolution to measure the strain distribution in axially heterostructured nanowires.

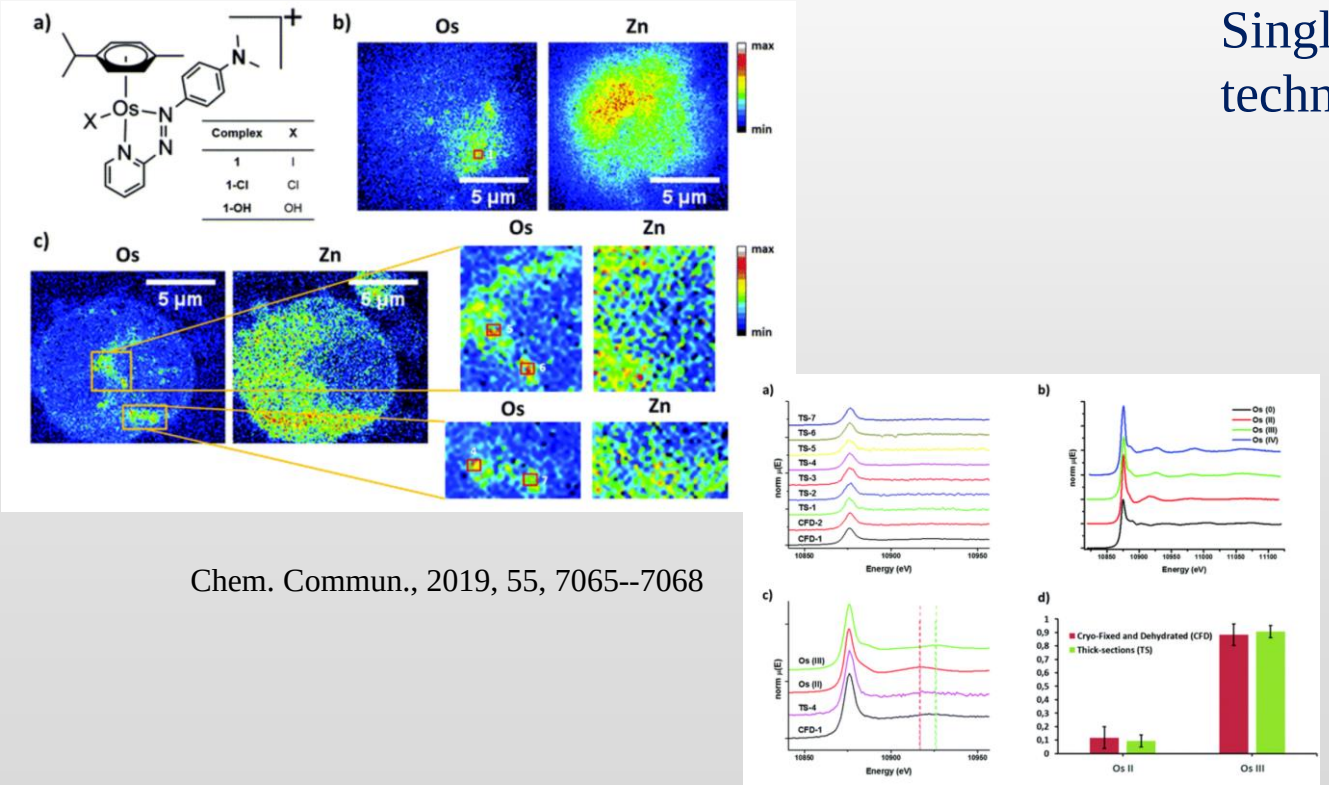




Application: Life Science

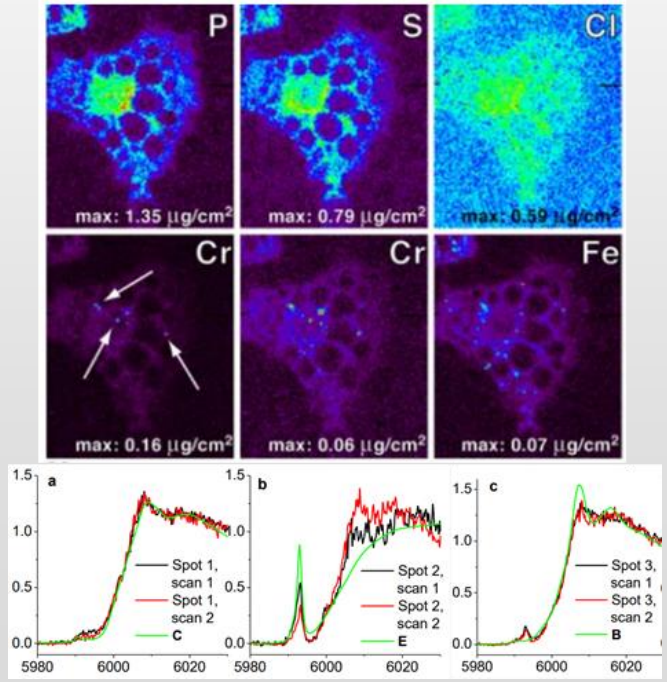
Nano-XRF and Nano-XANES were used to study of a intracellular complex at subcellular resolution allow detection and quantification of element species, which are distributed heterogeneously in different areas of the cell.

Subcellular X-ray Spectroscopy in Cancer Cells



Chem. Commun., 2019, 55, 7065--7068

Single-cell mapping and XANES spectroscopic techniques

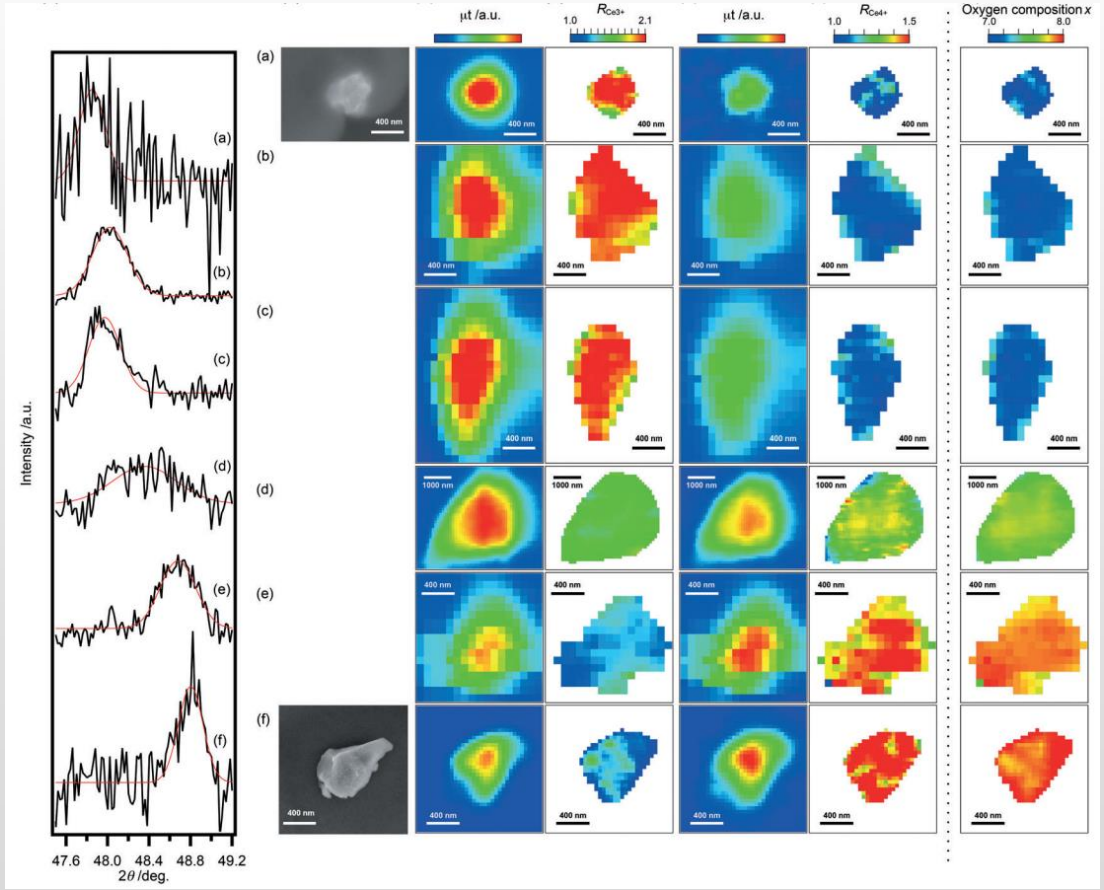


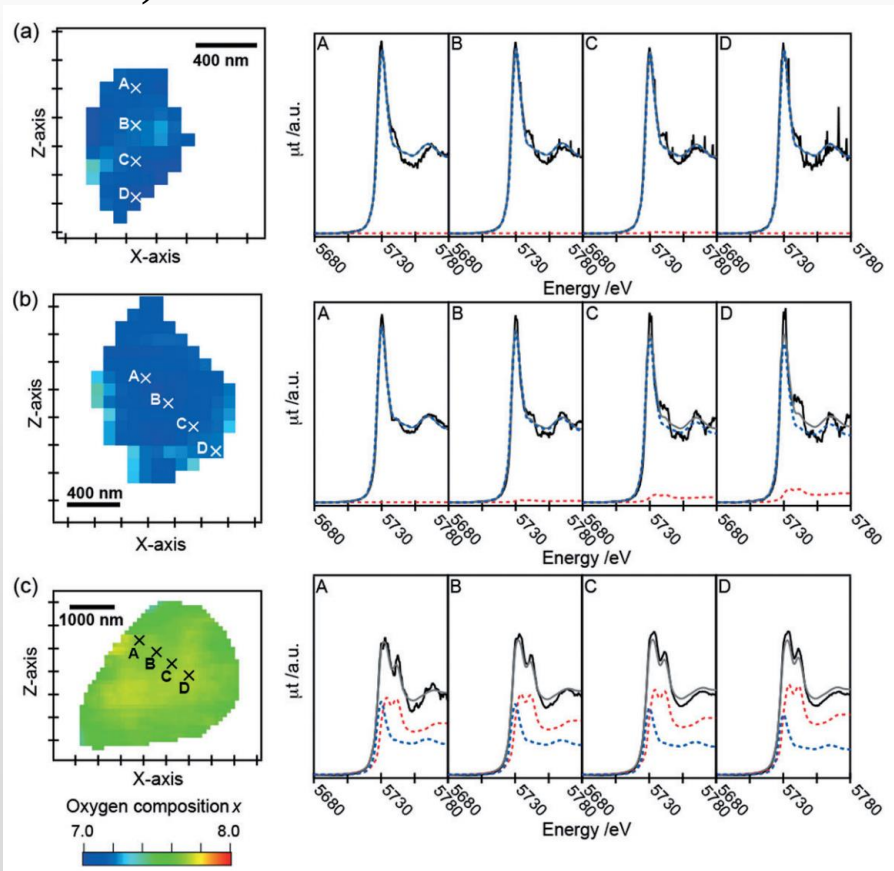
Angew. Chem., Int. Ed., 2016, 55, 1742

Application: Nano catalyst

Nano-XRF and Nano-XANES were used to visualize the heterogeneity of elemental oxidation states in single catalyst particles.

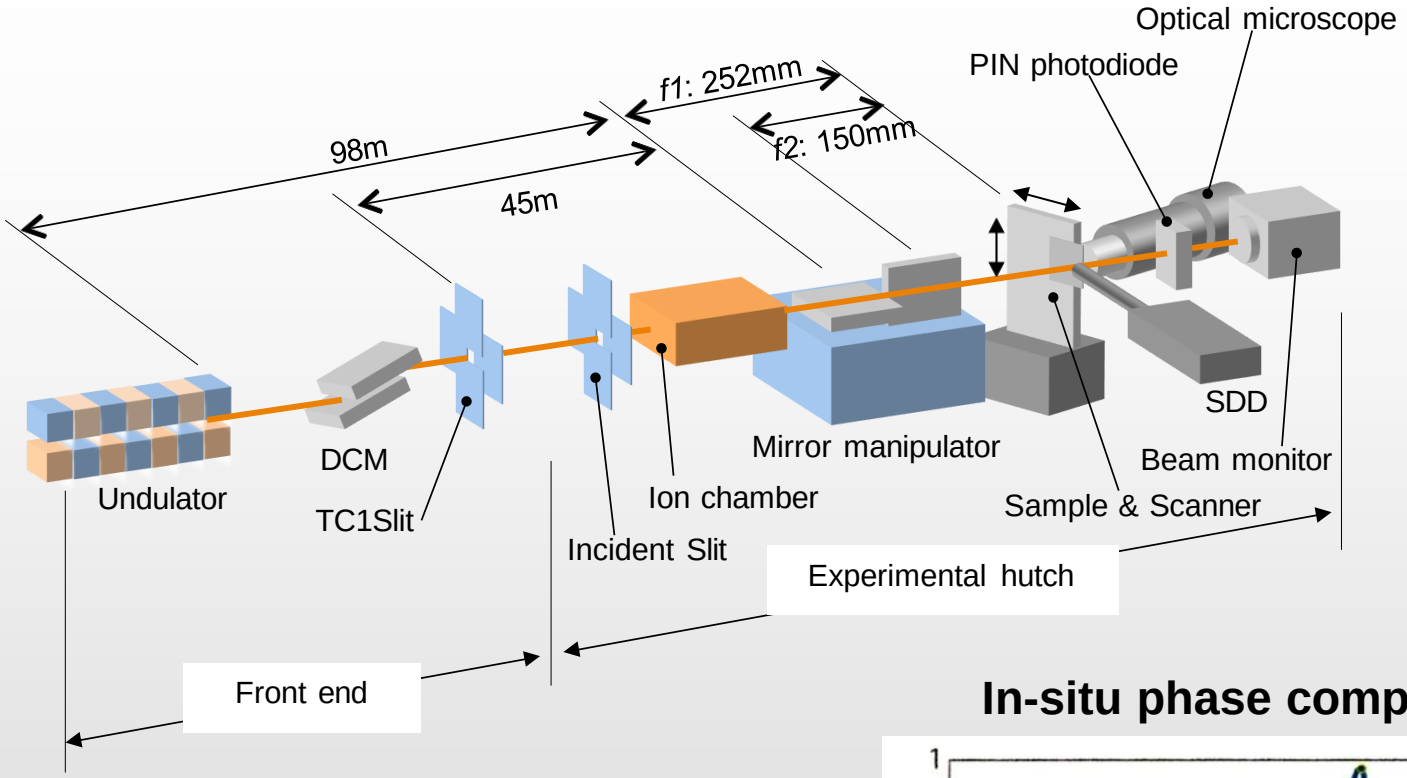
$Pt/Ce_2Zr_2O_x$ (x=7 to 8)



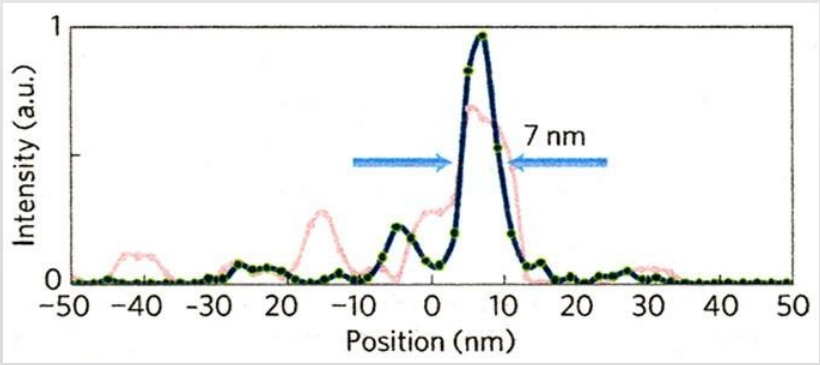


ChemPhysChem 2014, 15, 1563 – 1568

Hard x-ray nanoprobe at SPring-8



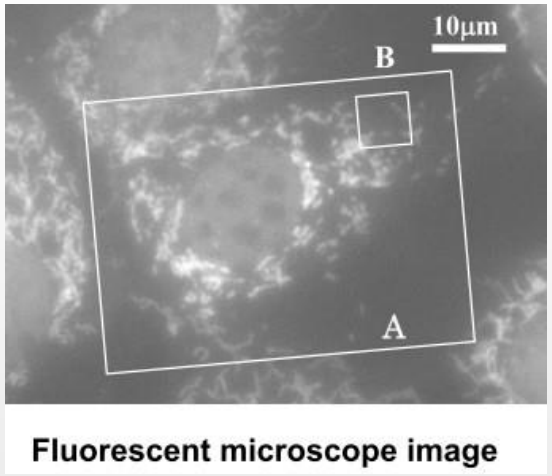
In-situ phase compensation

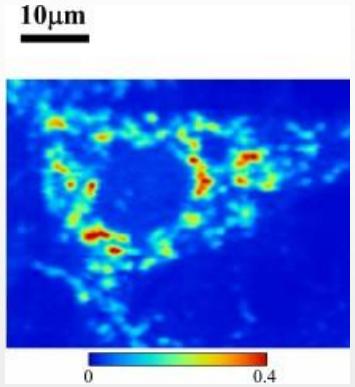


H. Mimura et al., *Nature Physics*, **6**, 122 (2009)

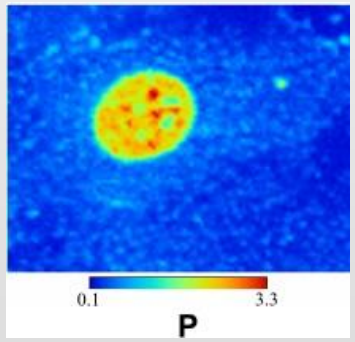
Courtesy of H. Mimura and
K. Yamauchi, Osaka University.

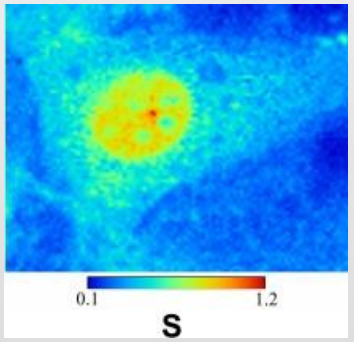
Hard x-ray nanoprobe at SPring-8

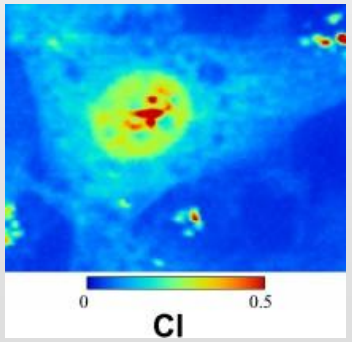


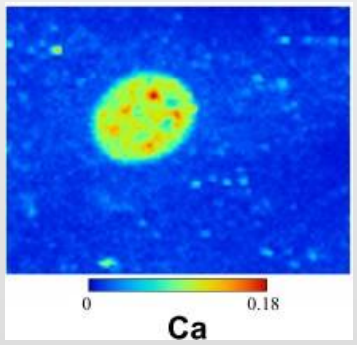


Sub-cellular elemental analysis using the hard x-ray fluorescence nanoprobe at SPring-8





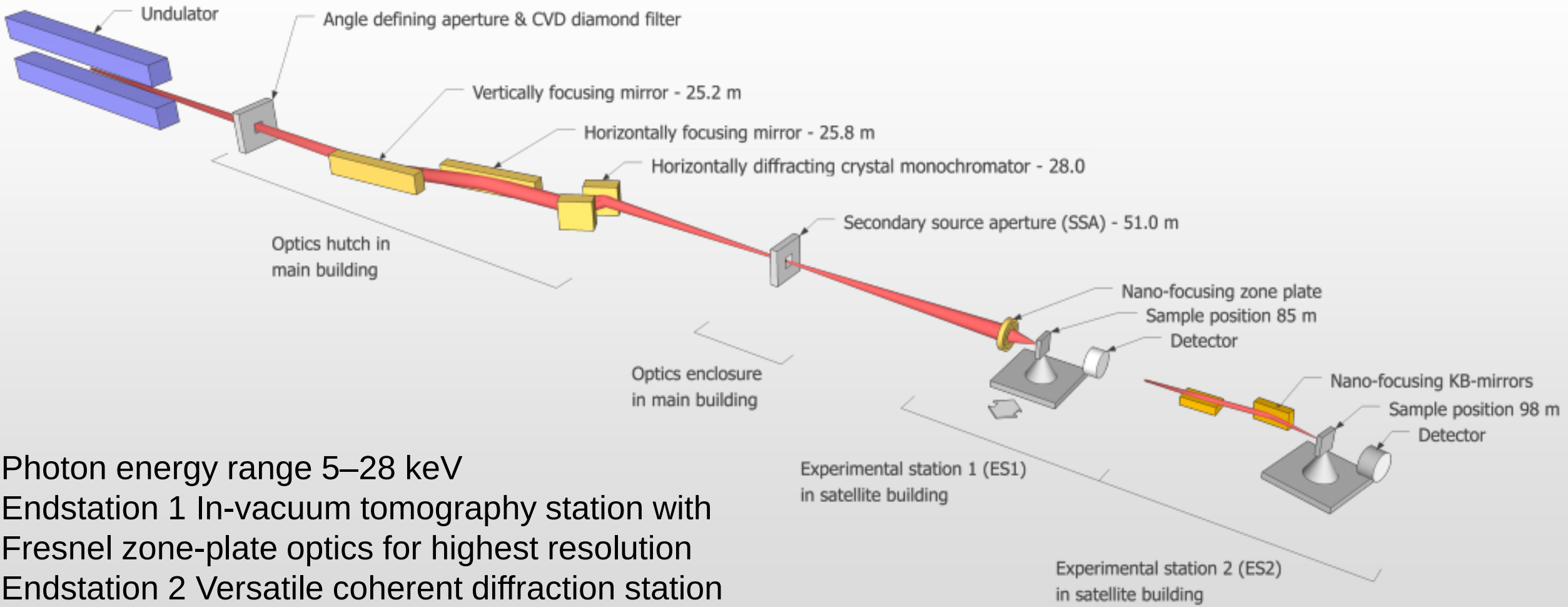




Courtesy of S. Matsuyama and
K. Yamauchi, Osaka University.

S. Matsuyama et al.,
X-Ray Spectrom.(2010).

NanoMAX



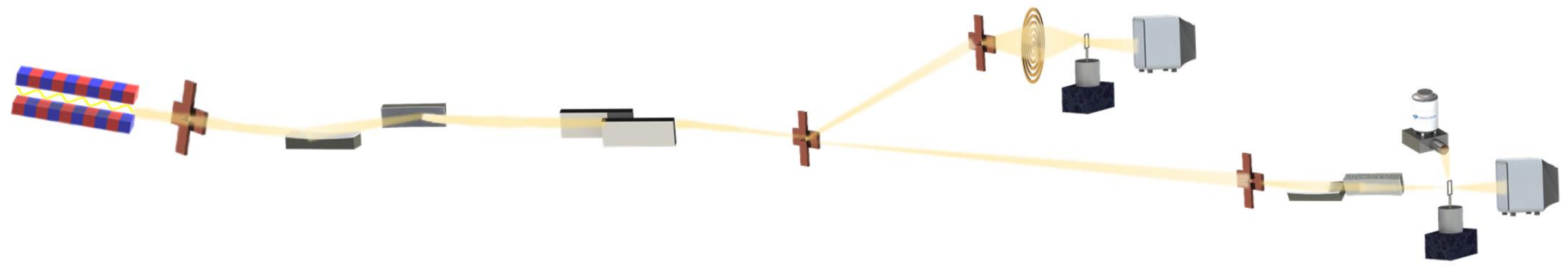
Photon energy range 5–28 keV
Endstation 1 In-vacuum tomography station with Fresnel zone-plate optics for highest resolution
Endstation 2 Versatile coherent diffraction station with KB optics

Nanoprobe beam-SILF

深圳综合粒子设施研究院
Institute of Advanced Science Facilities, Shenzhen

Key features

- Nanoscale spatial resolution
- Ultra-sensitive detection



Light source	Undulator
Energy range (keV)	5 ~ 22
Energy resolution (@10keV)	2×10^{-4}
Flux at 10 keV (ph/s)	1×10^{9} (EH1) 2×10^{10} (EH2)
Spot size at sample (nm)	~30 (EH1) ~100 (EH2)
Key features	Space resolution: ≤ 100 nm Detection limit: ppb

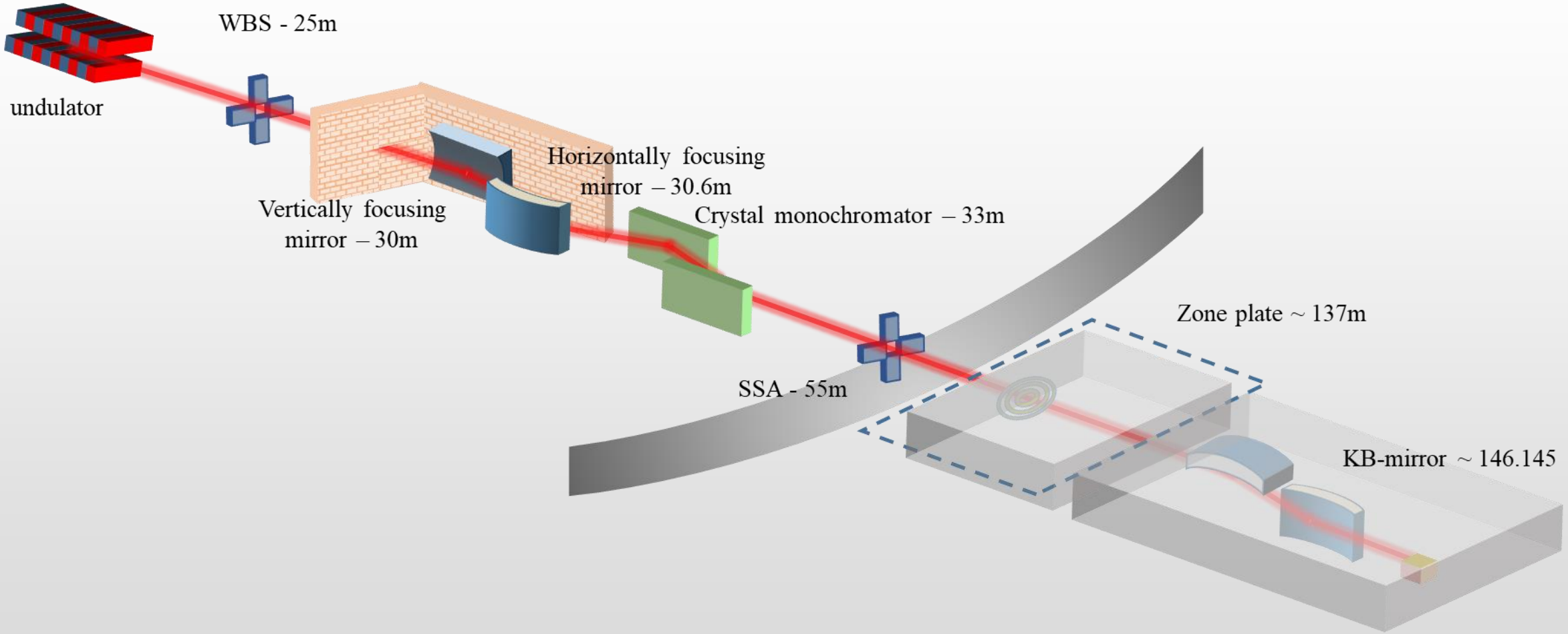
Method

- Nano-XRF
- Nano-XAFS
- Nano-XRD
- Ptychography
- Integrated

Applications

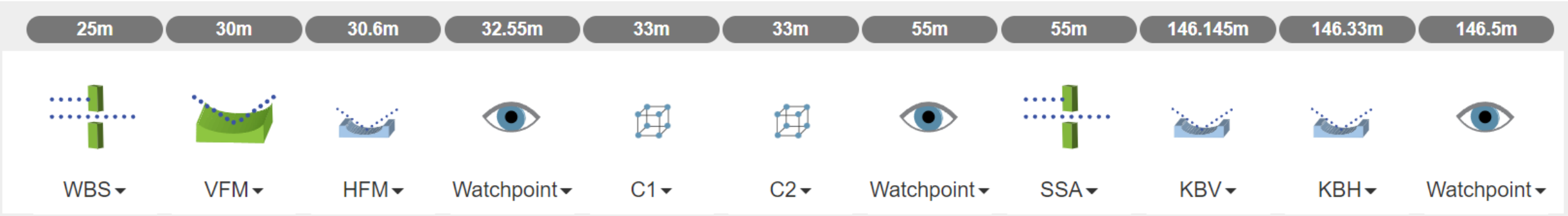
- Energy materials
- Nanoelectronics
- Life sciences
- Nanocatalyst

Beamline Optics-SILF

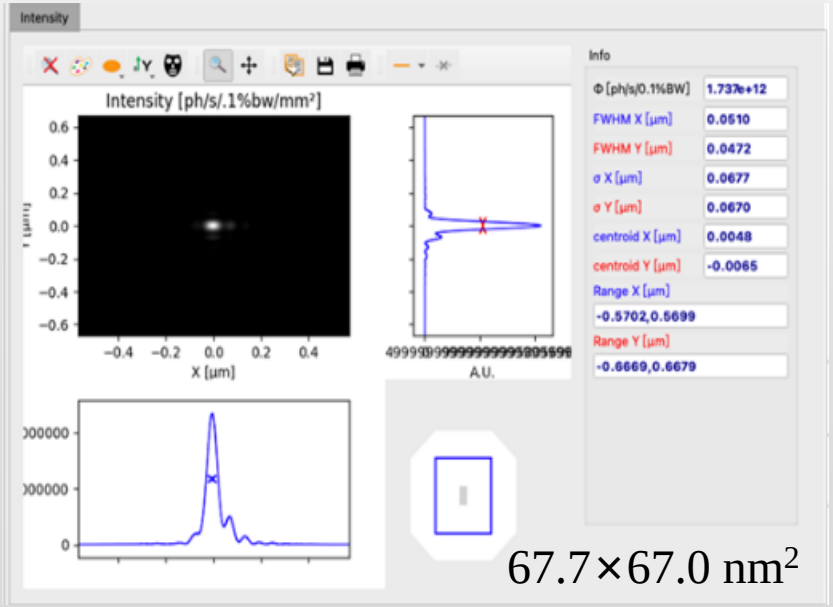


X-ray Tracing-SILF

深圳综合粒子设施研究院
Institute of Advanced Science Facilities, Shenzhen

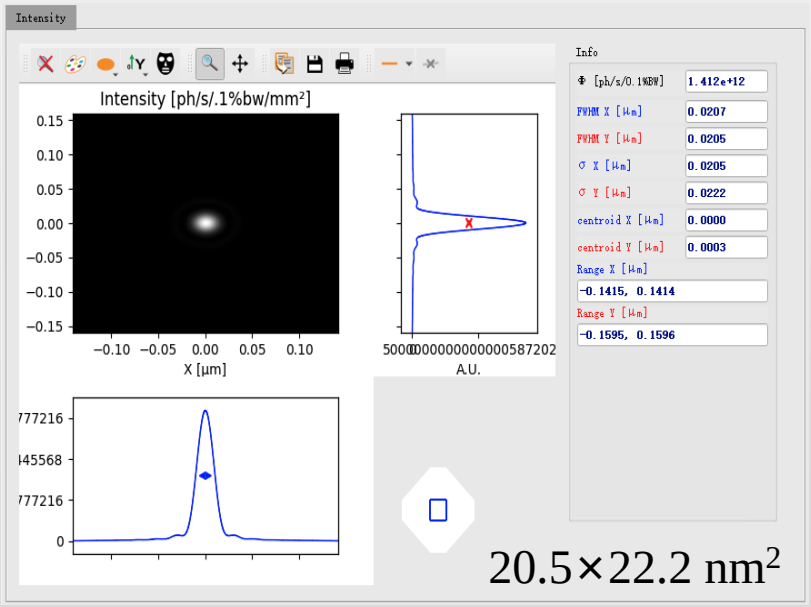


Simulation Result



67.7×67.0 nm²

Simulation Result

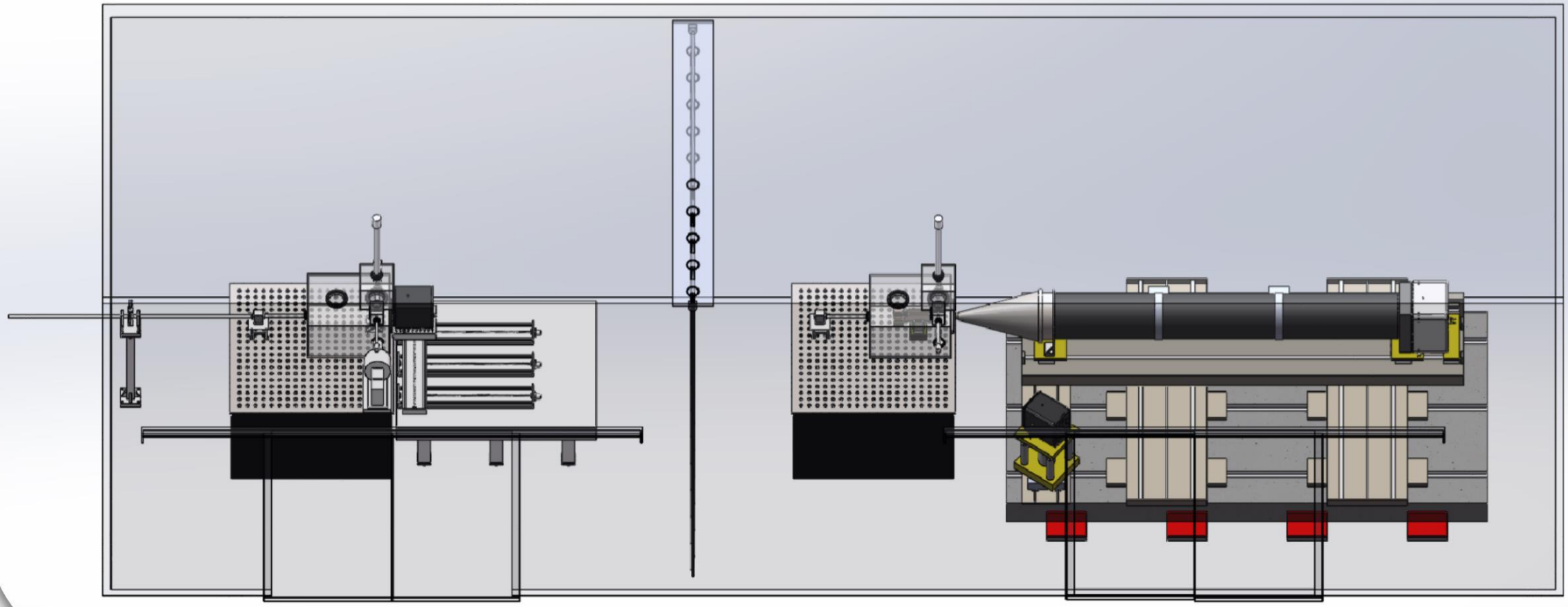


20.5×22.2 nm²

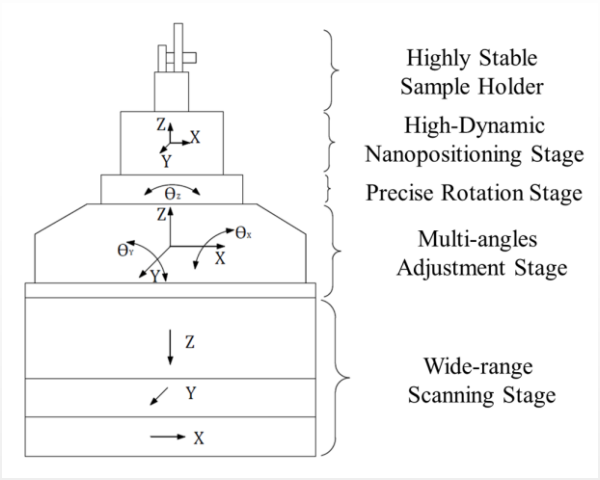
Experimental Hutch-SILF

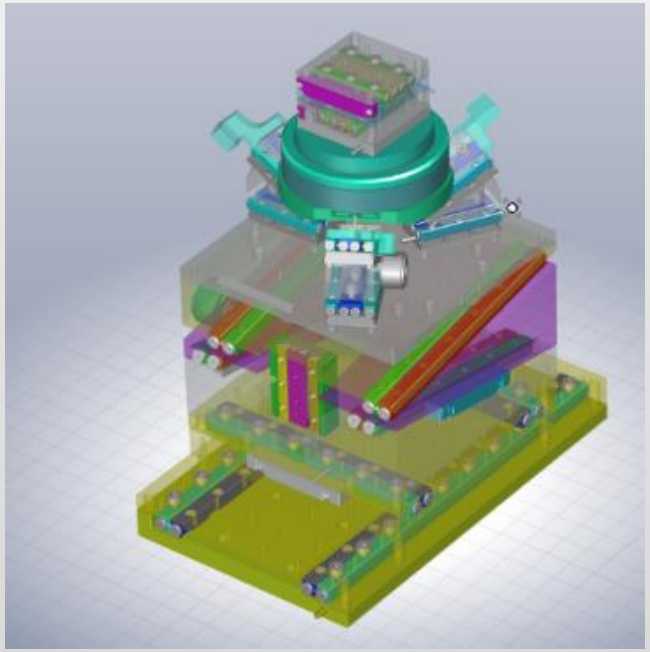
Endstation 1

Endstation 2



Instruments-SILF



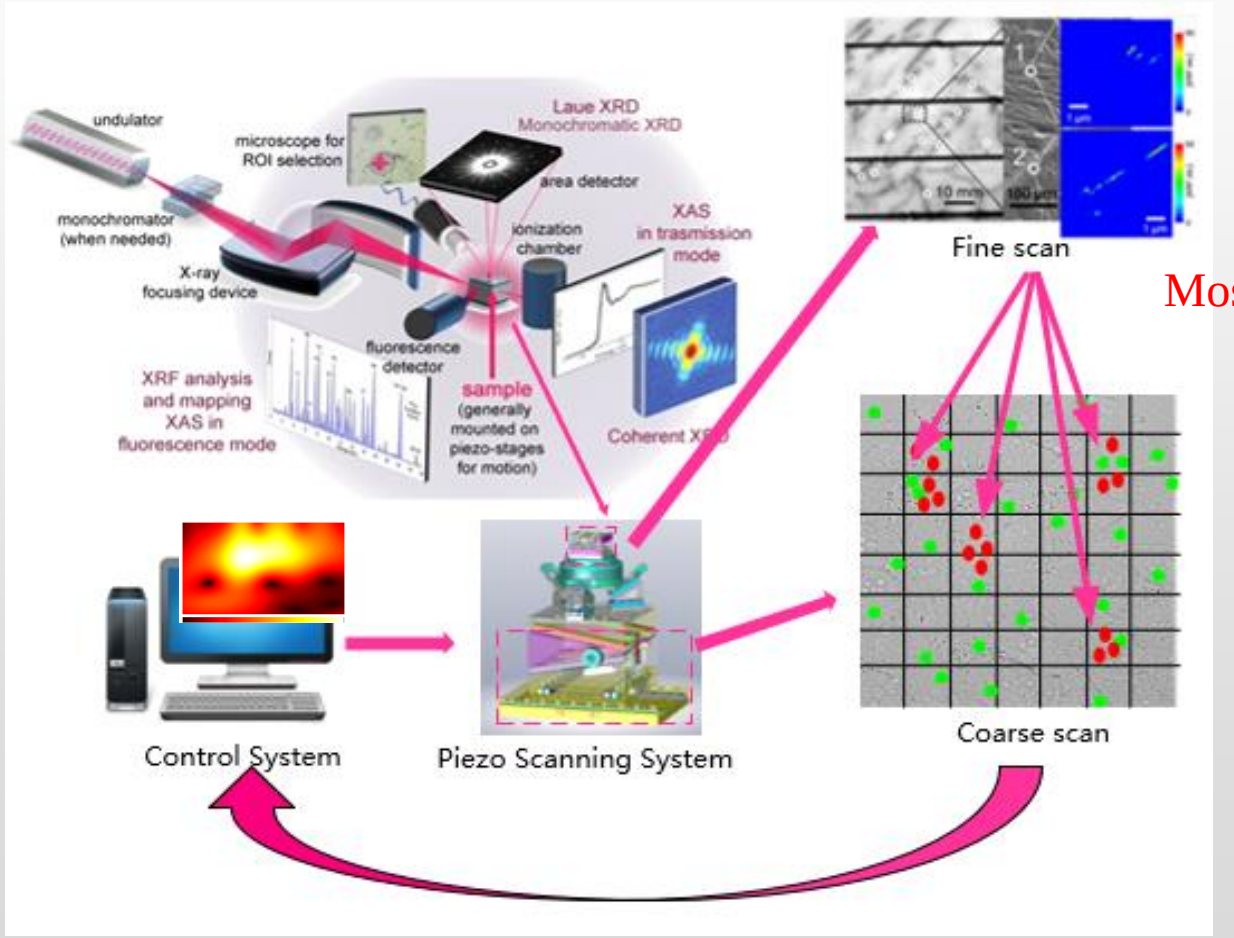


Sample stage: 9-Axis system with coarse and fine X, Y, Z and θx, θy, θz

Stages	Dimension	Range	Resolution	Accuracy	Load
High-Dynamic Nanopositioning Stage	X	100μm	< 1nm	±2.5nm	200g
	Y	100μm	< 1nm	±2.5nm	
	Z	100μm	< 1nm	±2.5nm	
Precise Rotation Stage	θ_Z	360°	15μrad	150μrad	> 500g
Multi-angles Adjustment Stage	θ_X	±5mrad	1μrad	±10μrad	> 800g
	θ_Y	±5mrad	1μrad	±10μrad	
Wide-range Scanning Stage	X	20mm	1nm	±100nm	> 1kg
	Y	20mm	1nm	±100nm	
	Z	20mm	1nm	±100nm	

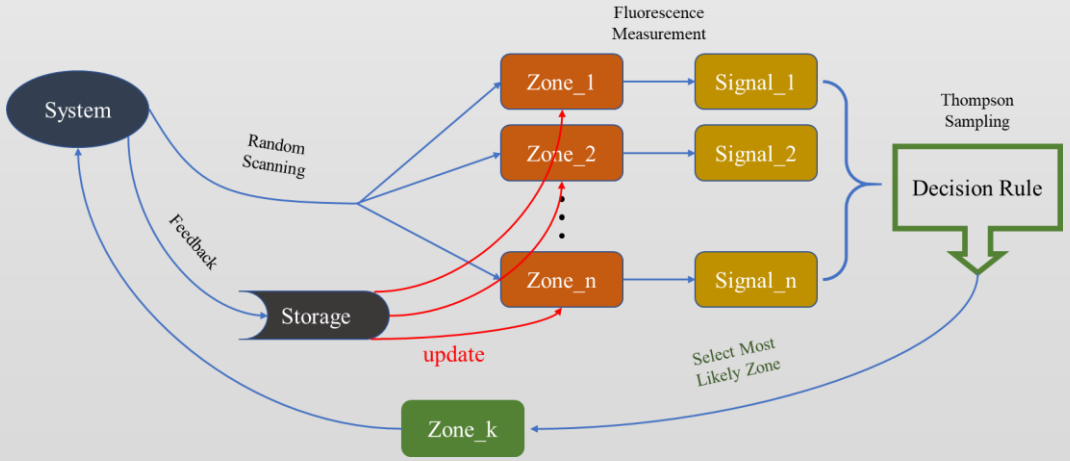
Instruments-SILF

The nanoprobe scanning system based on 9-axis sample stage and AI-based “multi-arm bandit” algorithm



Most likely sample regions

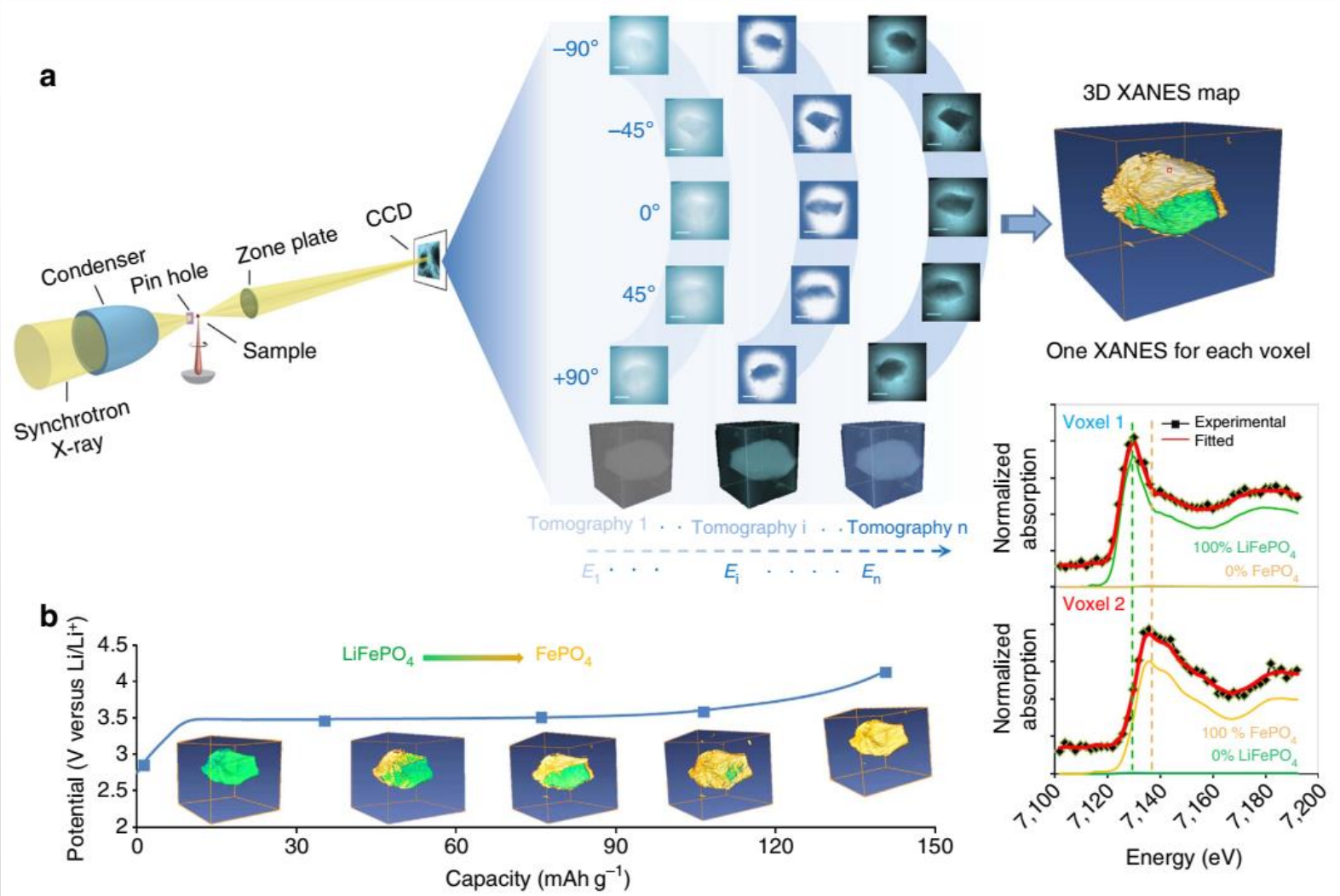
➢ Multi-arm Bandit Algorithm



Full-field Transmission X-ray Microscopes，TXM

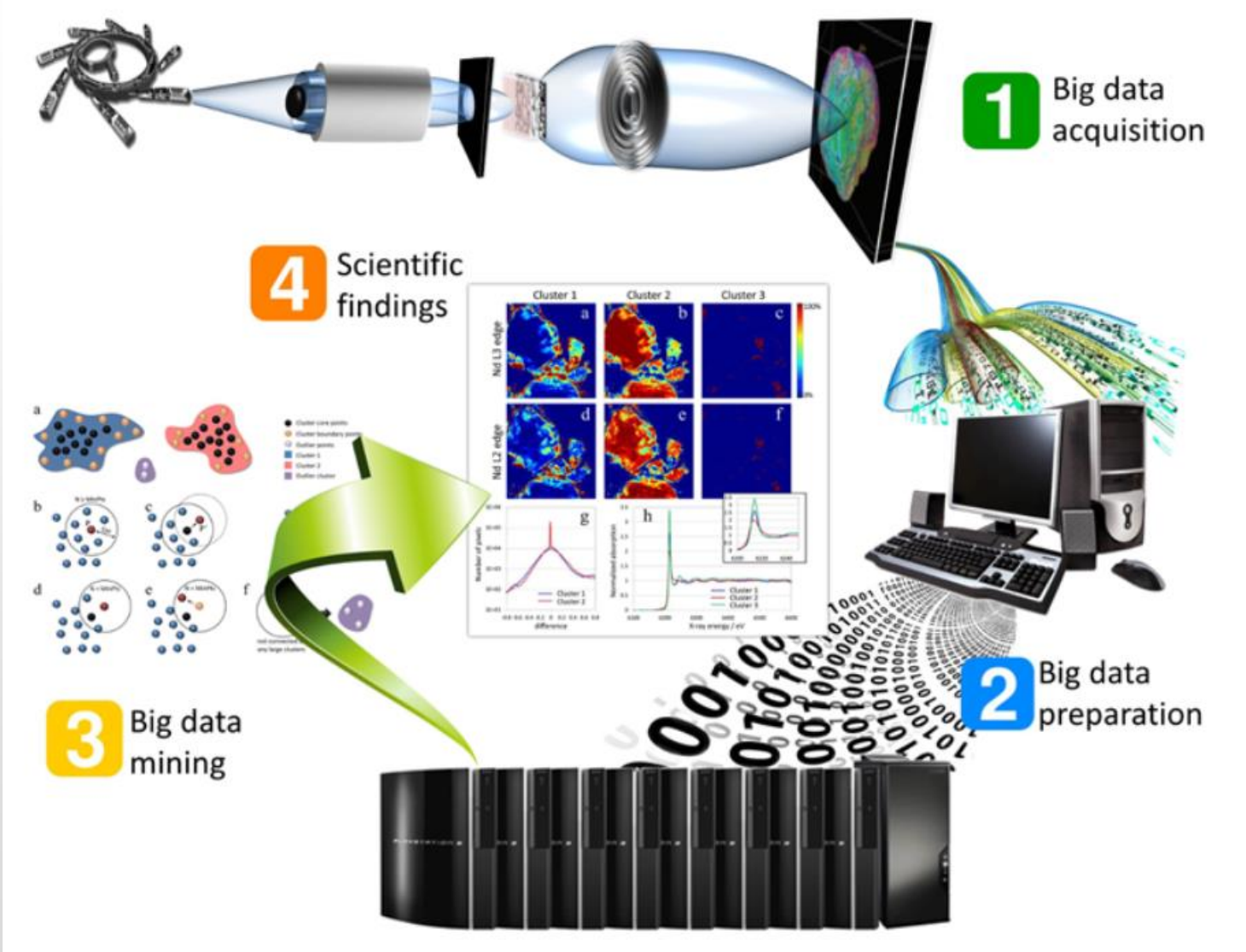


TXM - XANES



Nat Commun 7, 12372 (2016).

Data collection and processing process

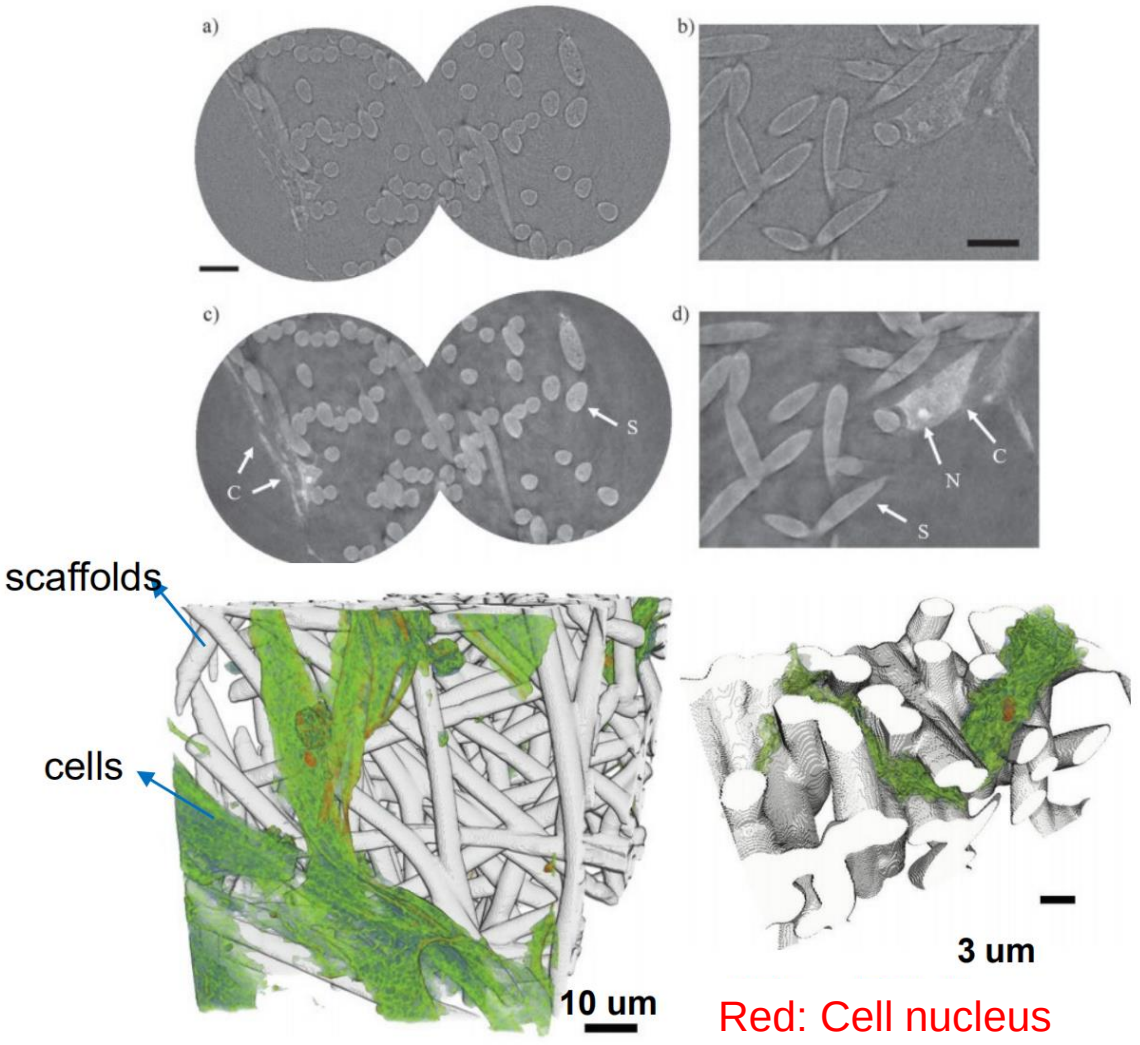


Applications

Life Science

3D X-Ray Nanotomography of Cells Grown on Electrospun Scaffolds

Using TXM-CT technology to observe the growth of cell tissue on biological stents, the growth of cells inside the bracket can be clearly observed. This is of great significance for the study of biomagmatic compatibility of implanted medical polymer materials.



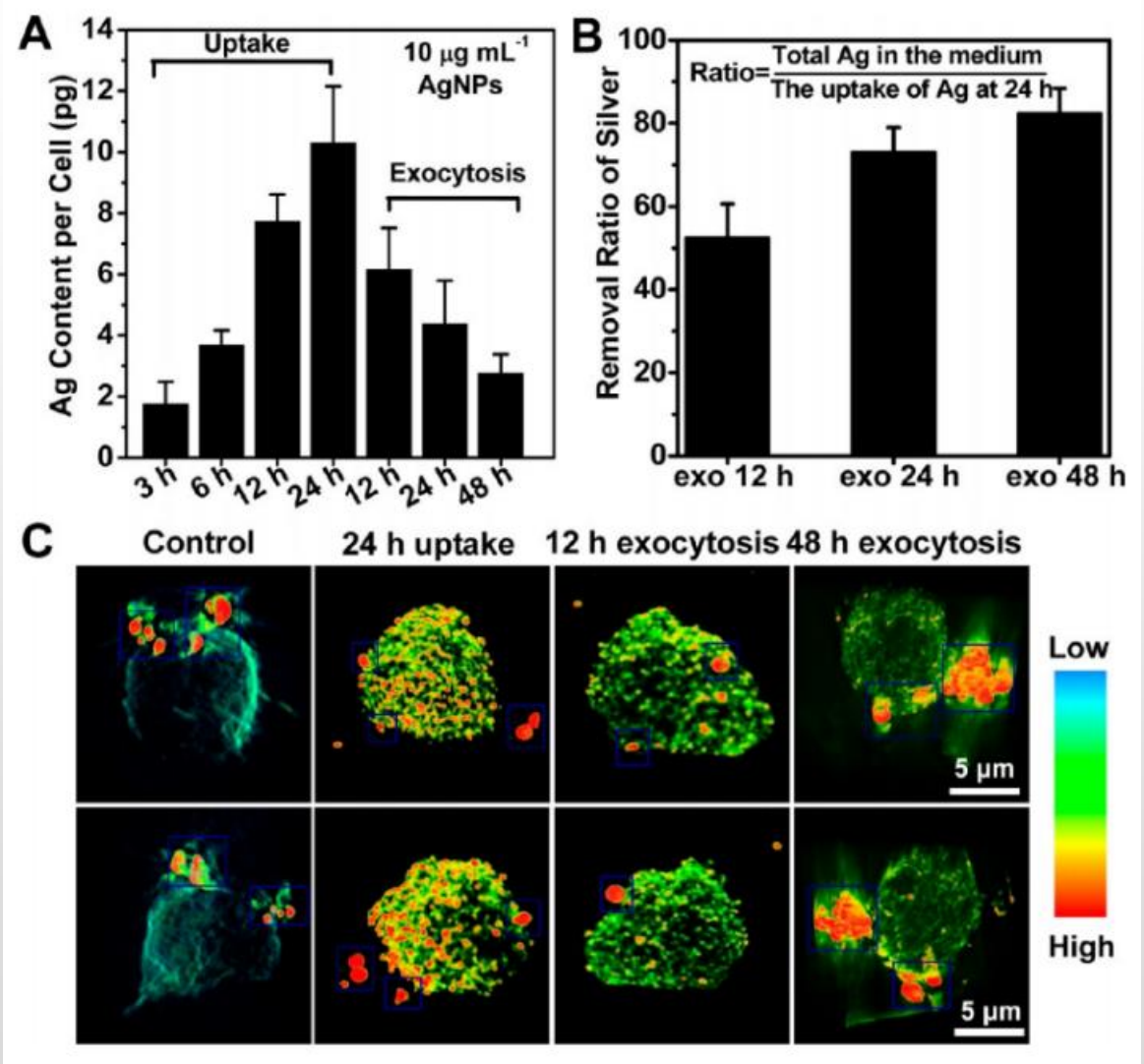
3D renderings of a into a scaffold after culturing for 3 d(left, the whole) and 6 d(right, cell grows in at ~43 um depth)

Applications

Life Science

Use of Synchrotron Radiation-Analytical Techniques To Reveal Chemical Origin of Silver-Nanoparticle Cytotoxicity

Beijing synchronous radiation device 4W1A-X-ray imaging experiment station uses TXM and near-side absorption spectrum to obtain the distribution of nanoparticles in a single human cell and changes in the chemical state of nanoparticles. It has a new understanding of the cell toxicity of nanoparticles.



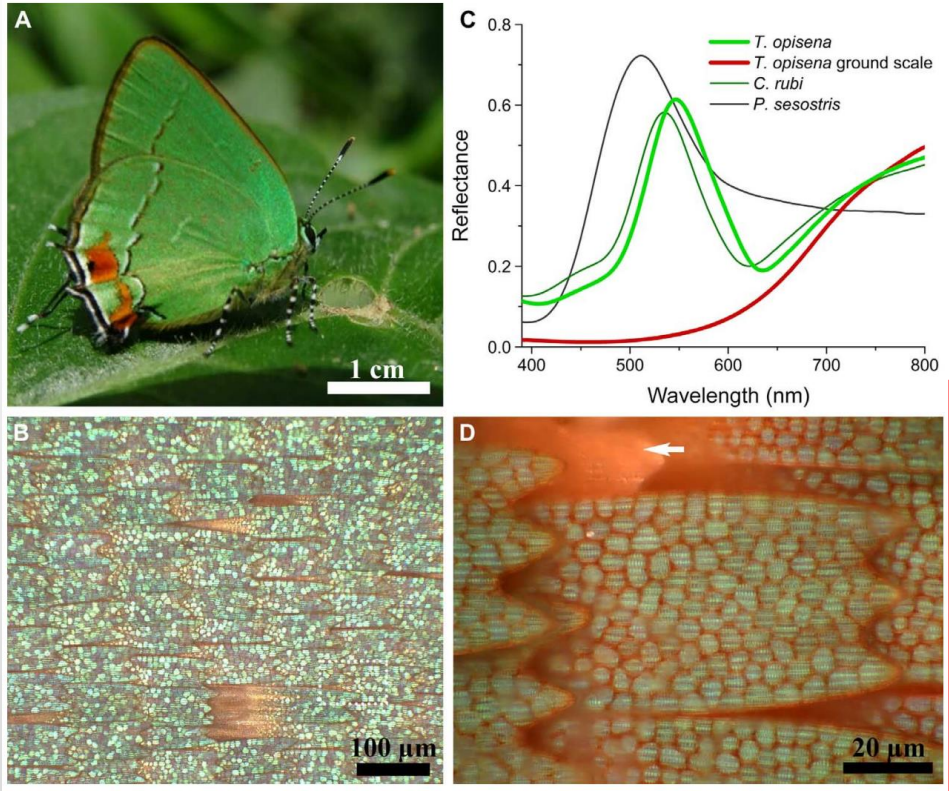
Applications

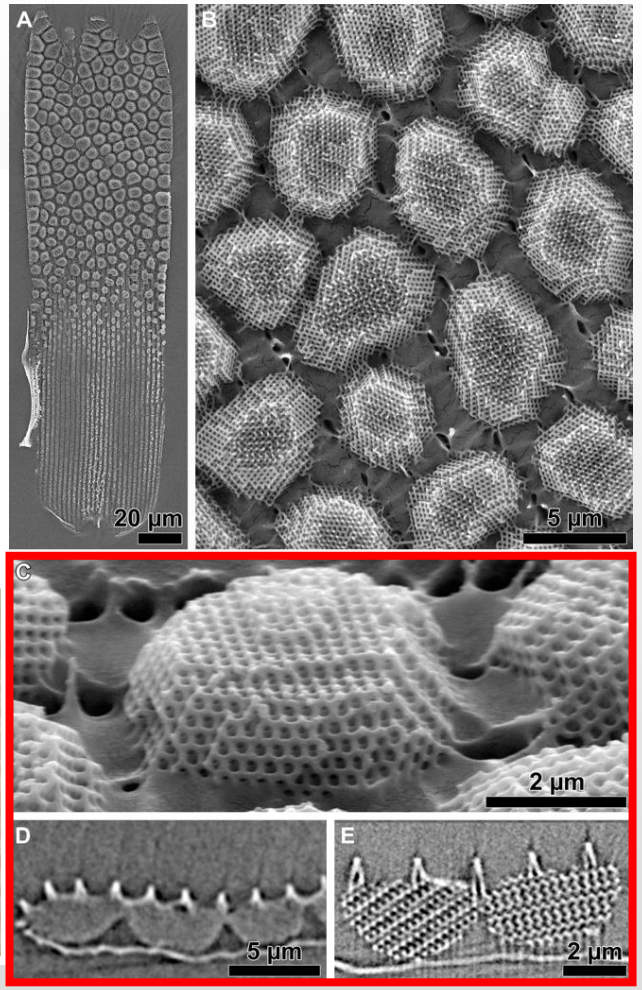
深圳综合粒子设施研究院
Institute of Advanced Science Facilities, Shenzhen

Life Science

Butterfly gyroid nanostructures as a time-frozen glimpse of intracellular membrane development

Use TXM-CT technology to observe the butterfly wings, you can clearly observe the photon crystal structure displayed. This is of great significance for the study of bionic learning Mica structural materials.





Reconstruction results of TXM-CT

Applications

Micro-nano structure material: internal structure of alloy

NSLS II 18-ID nano-imaging line:
Al-TIC's micro-structure observation. TXM-CT data observes the internal structure of Al-TIC.

Real-time visualization of particle evolution during reactive flux-assisted processing of aluminum melts. Scripta Mater., 201, 113978 (2021).

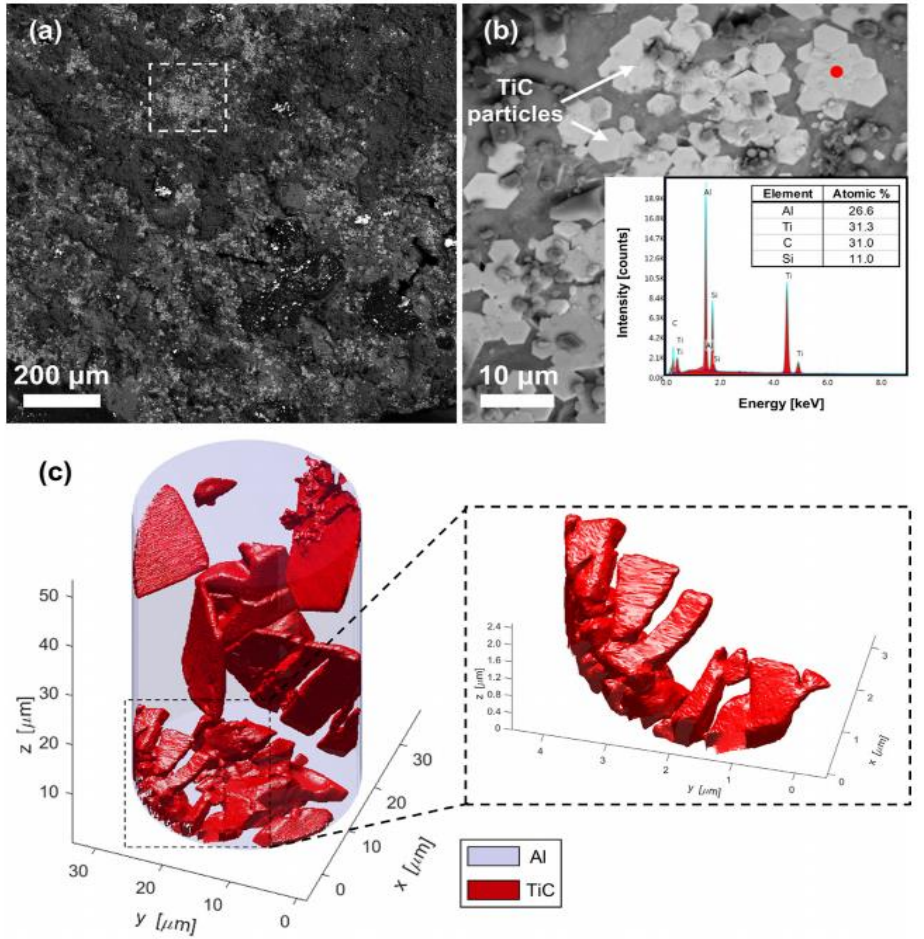


Fig. 3. Microstructural observations of the Al-TiC MMC reacted in the XRR experiments. (a) BSE SEM micrograph of the sample surface in the region corresponding to the XRR FOV. (b) Representative higher magnification BSE SEM image of the sample surface (corresponding to the boxed region in (a)) showing carbide particles/platelets. A spot EDS spectrum taken from the red dot in (b) is shown as an inset. (c) 3D volume rendering of reconstructed TXM data showing a cylindrical field-of-view with TiC particles/platelets (red) in an aluminum matrix (blue). A higher magnification rendering of a stepped, faceted particle is shown as an inset (c, right) (For interpretation of the references to color in this figure legend, the reader is referred to the web version of this article.).

Applications

Micro-nano structure material: molten salt micro structure evolution

NSLS II 18-ID nano imaging line station: Under 800 ° C, KCL-MGCL2 molten salt reaction X-ray nano-fault scan. Observed the formation of porous structures and the growth of related characteristics.

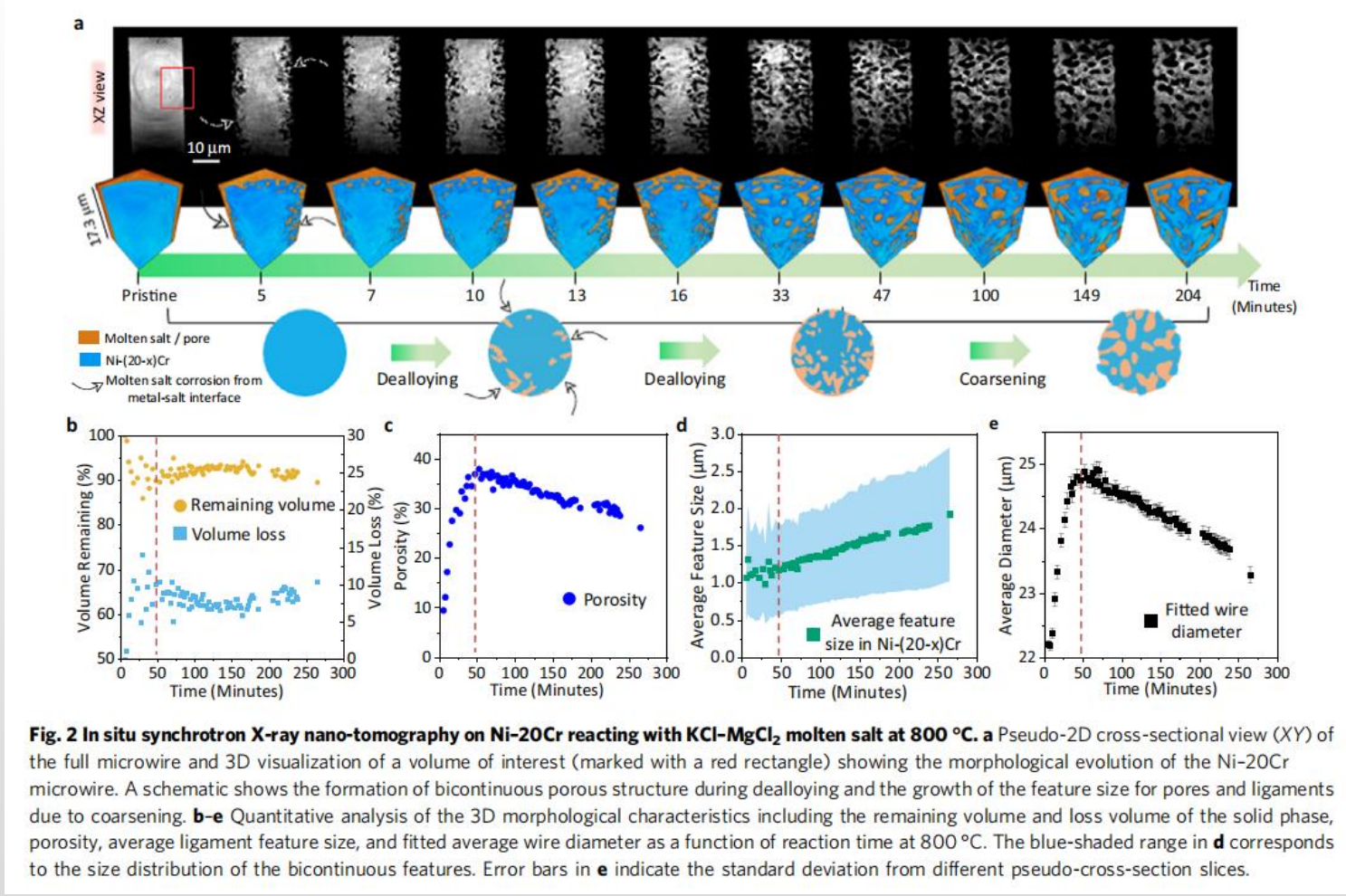


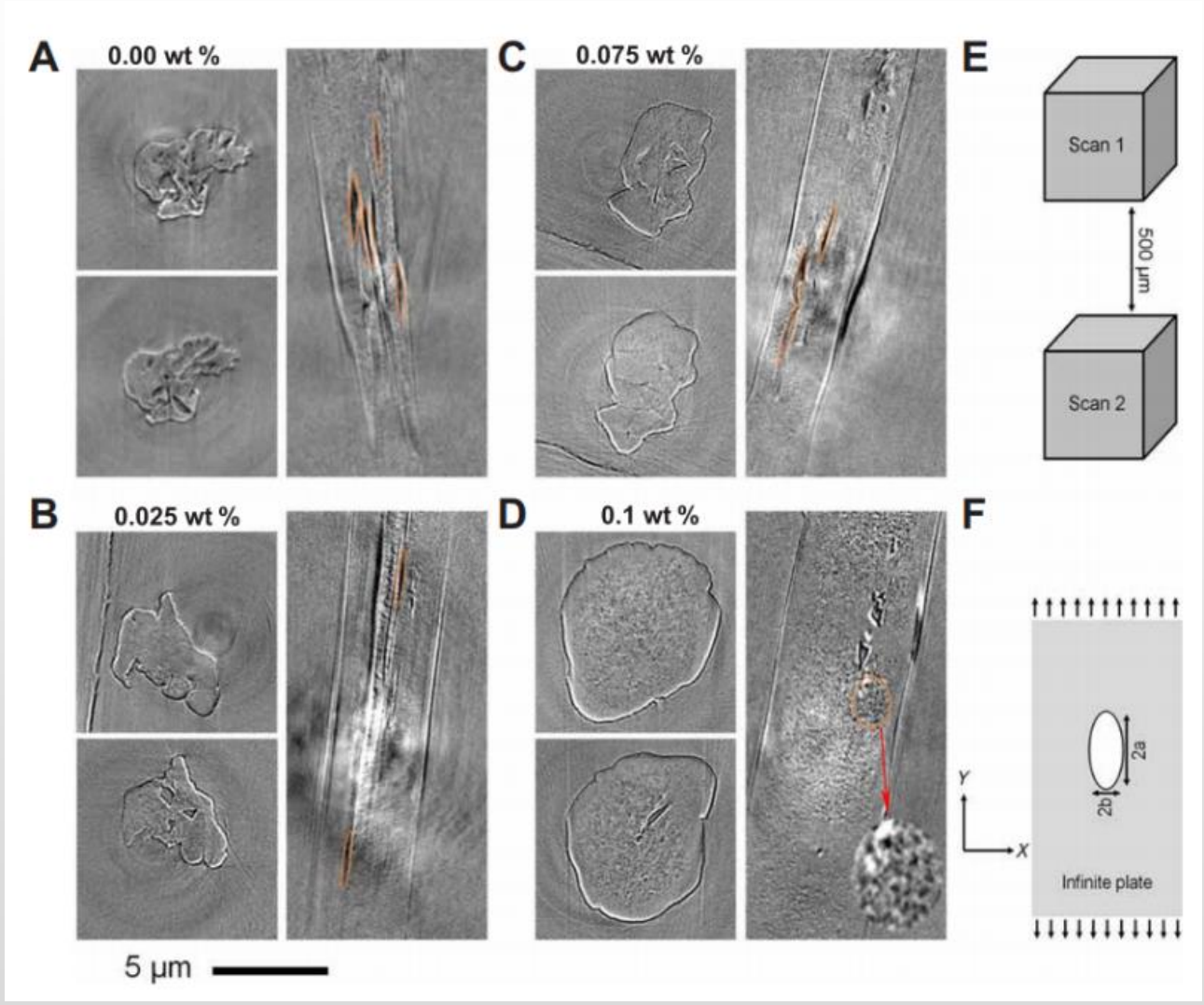
Fig. 2 In situ synchrotron X-ray nano-tomography on Ni–20Cr reacting with KCl–$MgCl_2$ molten salt at 800 °C. a Pseudo-2D cross-sectional view (*XY*) of the full microwire and 3D visualization of a volume of interest (marked with a red rectangle) showing the morphological evolution of the Ni–20Cr microwire. A schematic shows the formation of bicontinuous porous structure during dealloying and the growth of the feature size for pores and ligaments due to coarsening. **b–e** Quantitative analysis of the 3D morphological characteristics including the remaining volume and loss volume of the solid phase, porosity, average ligament feature size, and fitted average wire diameter as a function of reaction time at 800 °C. The blue-shaded range in **d** corresponds to the size distribution of the bicontinuous features. Error bars in **e** indicate the standard deviation from different pseudo-cross-section slices.

Formation of three-dimensional bicontinuous structures via molten salt dealloying studied in real-time by in situ synchrotron X-ray nano-tomography. Nat. Comm., 12(1) (2021).

Applications

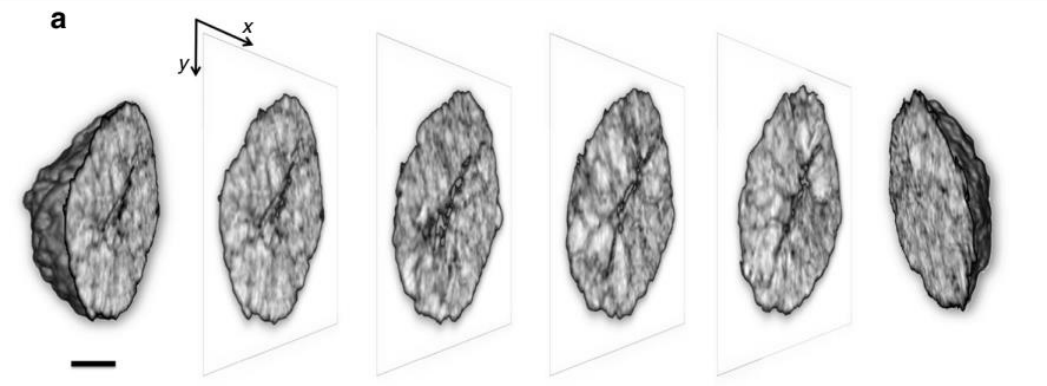
Micro-nano structure material: carbon fiber

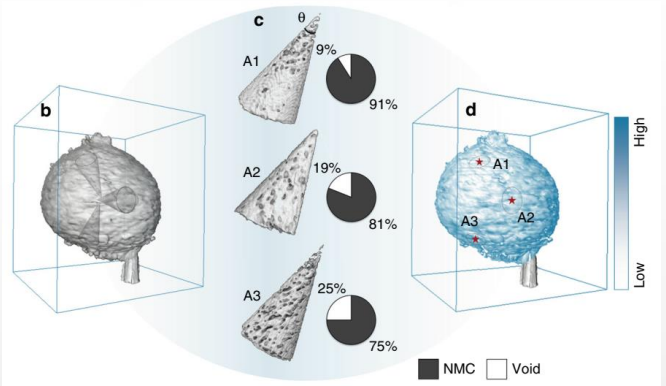
The NSLS II 18-ID nano-imaging line station: Studies the enhancement of graphene on carbon fiber. It is found that a small amount of graphene can reduce the pore rate/defect, and at the same time increase the amount and strength of the fiber.



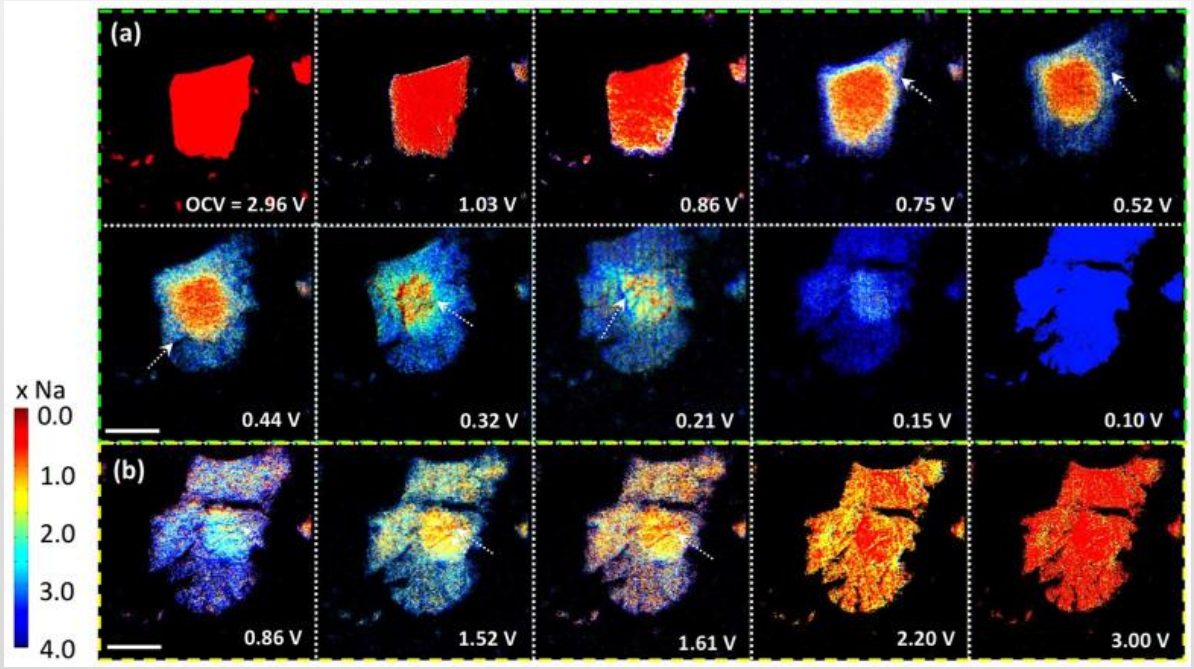
Graphene reinforced carbon fibers. Sci. Adv., 6(17), eaaz4191 (2020).

Applications





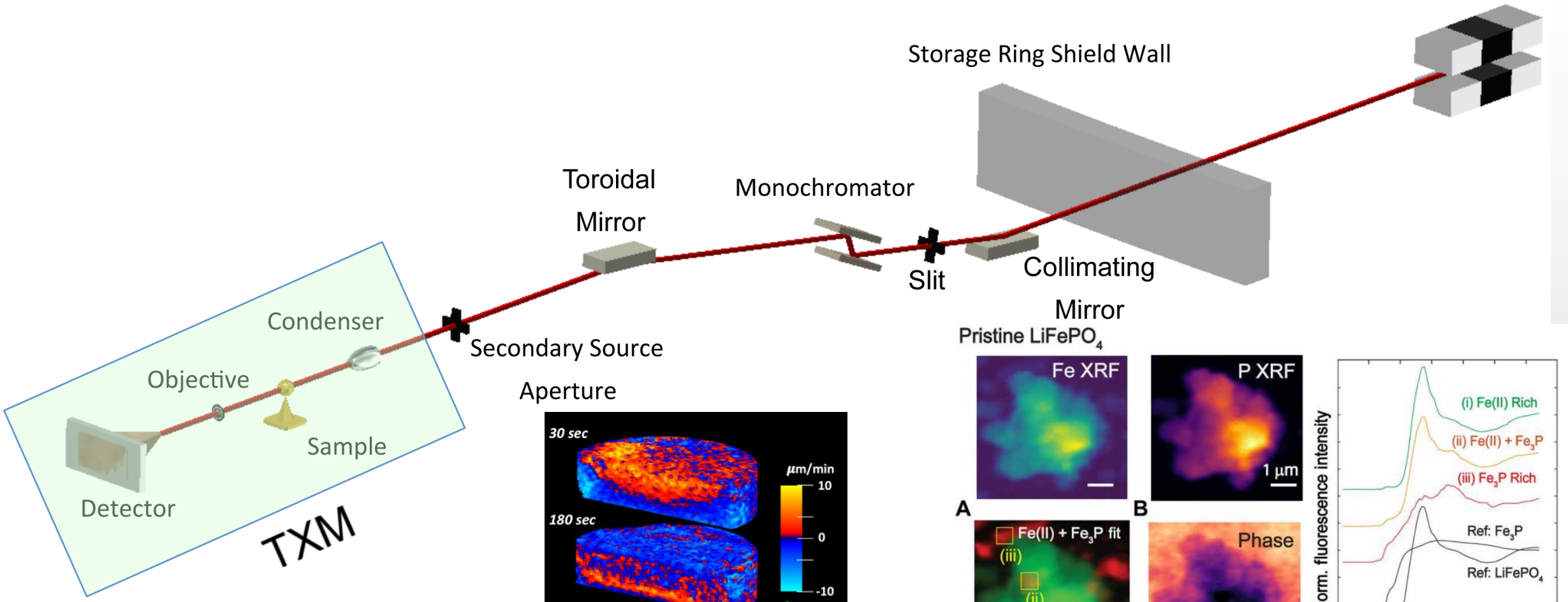
$LiNi_{0.8}Mn_{0.1}Co_{0.1}O_2$ (NMC811) Two granules X-ray nano-CT characteristics. Nat. Commun. ***11****, 4433 (2020).*



Two -dimensional chemical phase representation of lithium battery in the process Nano Energy 43, 184–191 (2018).

18-ID @NSLS II

深圳综合粒子设施研究院
Institute of Advanced Science Facilities, Shenzhen



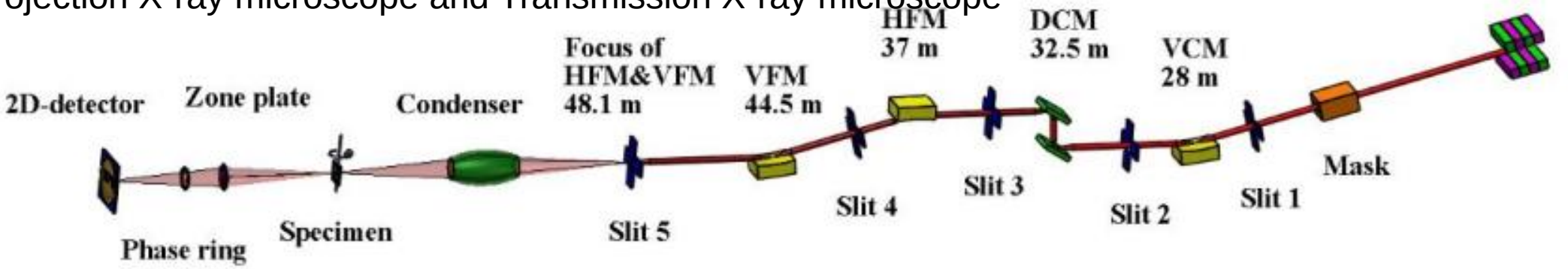
Study on the drying process in the preparation of lithium-ion battery cathodes

Chemical imaging of the pristine iron-rich phase using XANES TXM

31A@TPS

深圳综合粒子设施研究院
Institute of Advanced Science Facilities, Shenzhen

Projection X-ray microscope and Transmission X-ray microscope



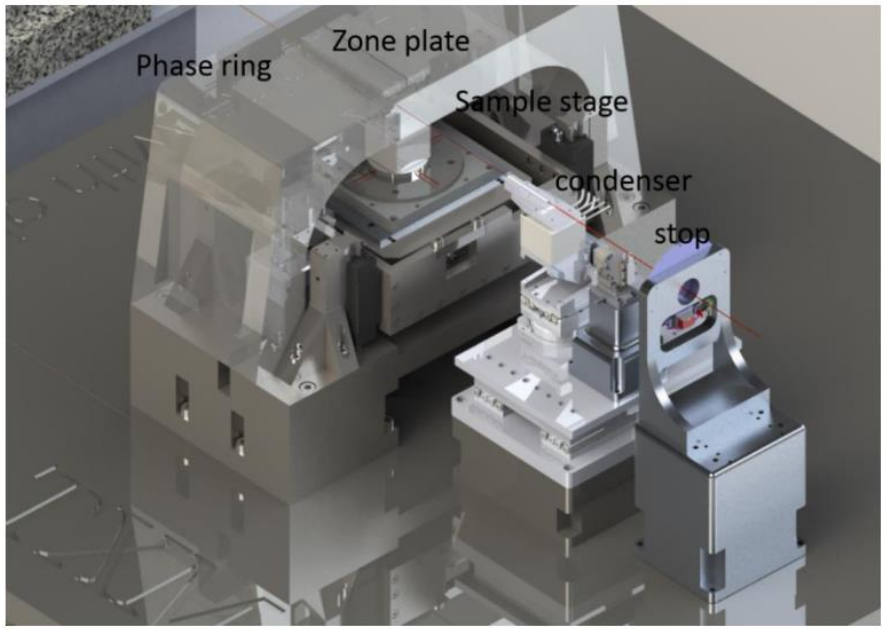


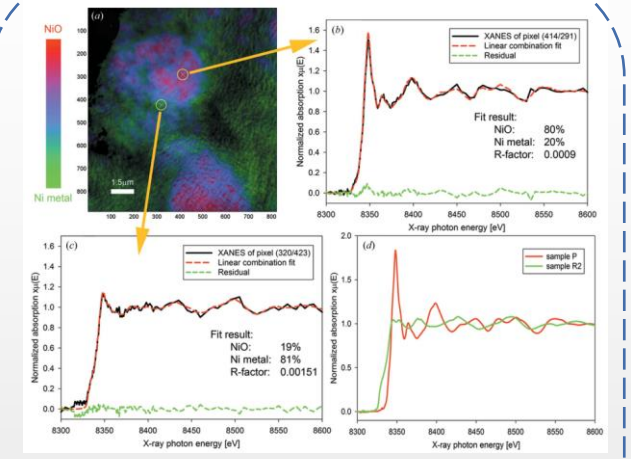
Figure 27. The conceptually design of the TXM module.

	FOV	Flux (photons/s) @ 10 keV	Energy resolution	Energy Range	Resolution
TXM	30 μm	2×10^{11}	1.4×10^{-4}	5-12 keV	30 nm

In order to use the beam efficiently, a pair of focusing mirrors was installed. A horizontal focusing mirror (HFM) and vertical focusing mirror (VFM) were placed behind the DCM so that the beam can focus on the secondary source, followed by refocusing by the capillary condenser on the sample position. Table shows the calculated flux for the absorption condenser. The beam on the sample is reshaped by the condenser, which has a hollow-cone shape and is well matched with the numerical aperture of the zoneplate.

TXM beamline-SILF

- Full-Field Transmission X-ray Microscopy Imaging (TXM)
- X-ray Absorption Near Edge Structure (XANES)
- X-ray Fluorescence (XRF)



XANES Spectroscopic Analysis

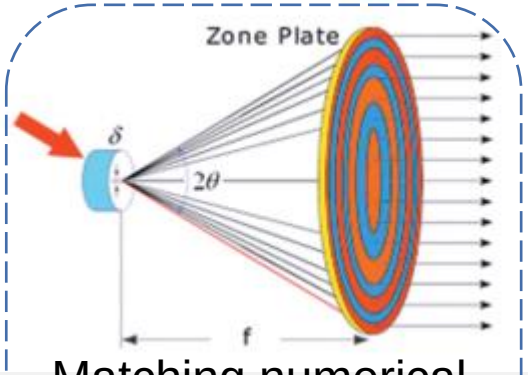
Principles of Beamline Design

Energy resolution
2e-4@8keV

Larger phase space of beam
100um-mrad

Energy range covering
5-11keV

Maximizing photon flux at sample position

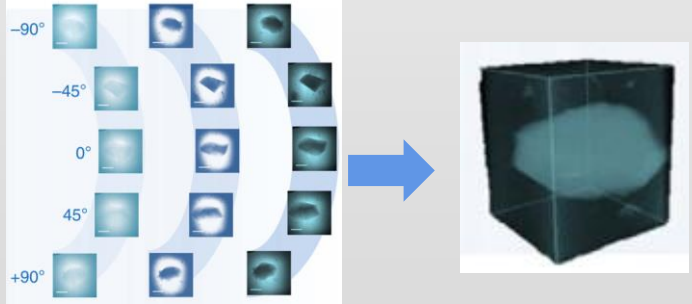


Matching numerical aperture of the zone plate



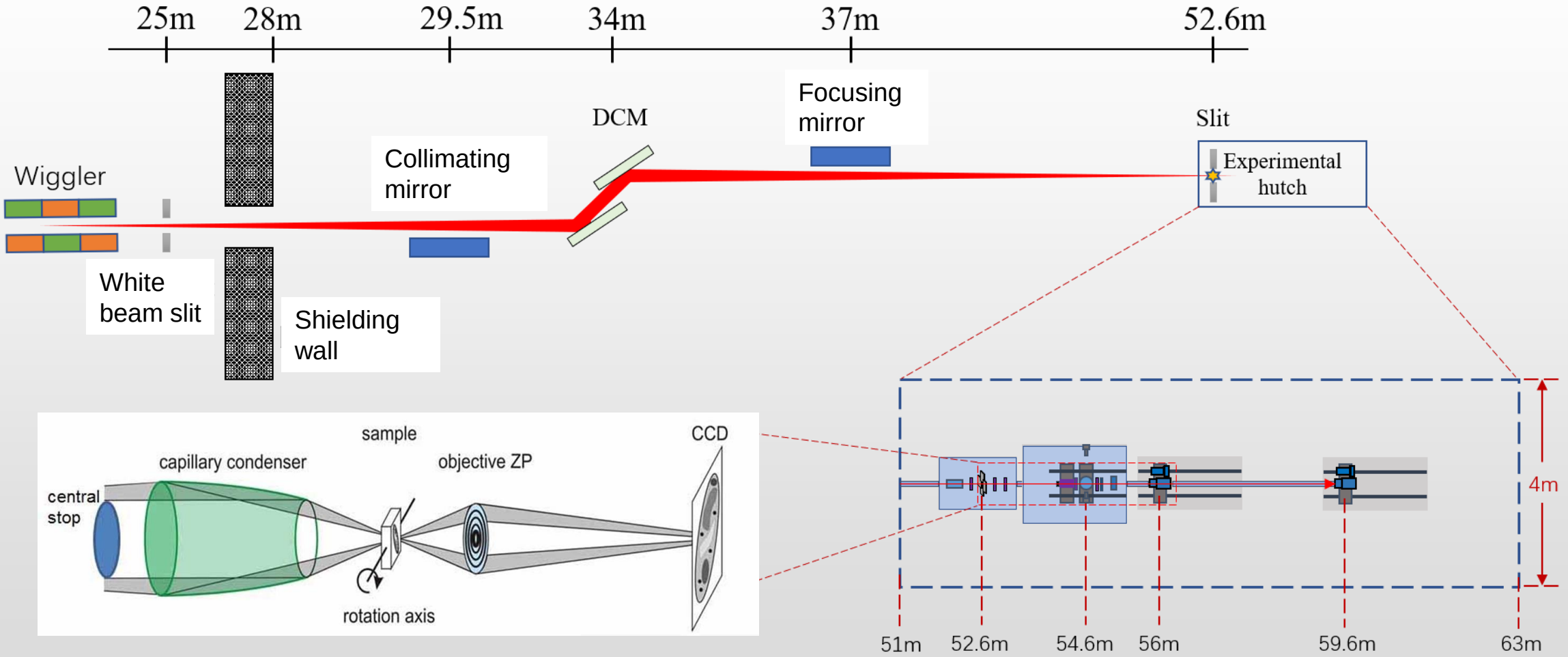
The efficiency of zone plate is higher in the energy range below 11 keV, which covers the main elements of battery materials

- Imaging mechanism: absorption, phase contrast
- Energy range: 5-11 keV
- Field of view: ≥ 20 μm
- Spatial resolution： 30nm
- Structure, chemical information etc.

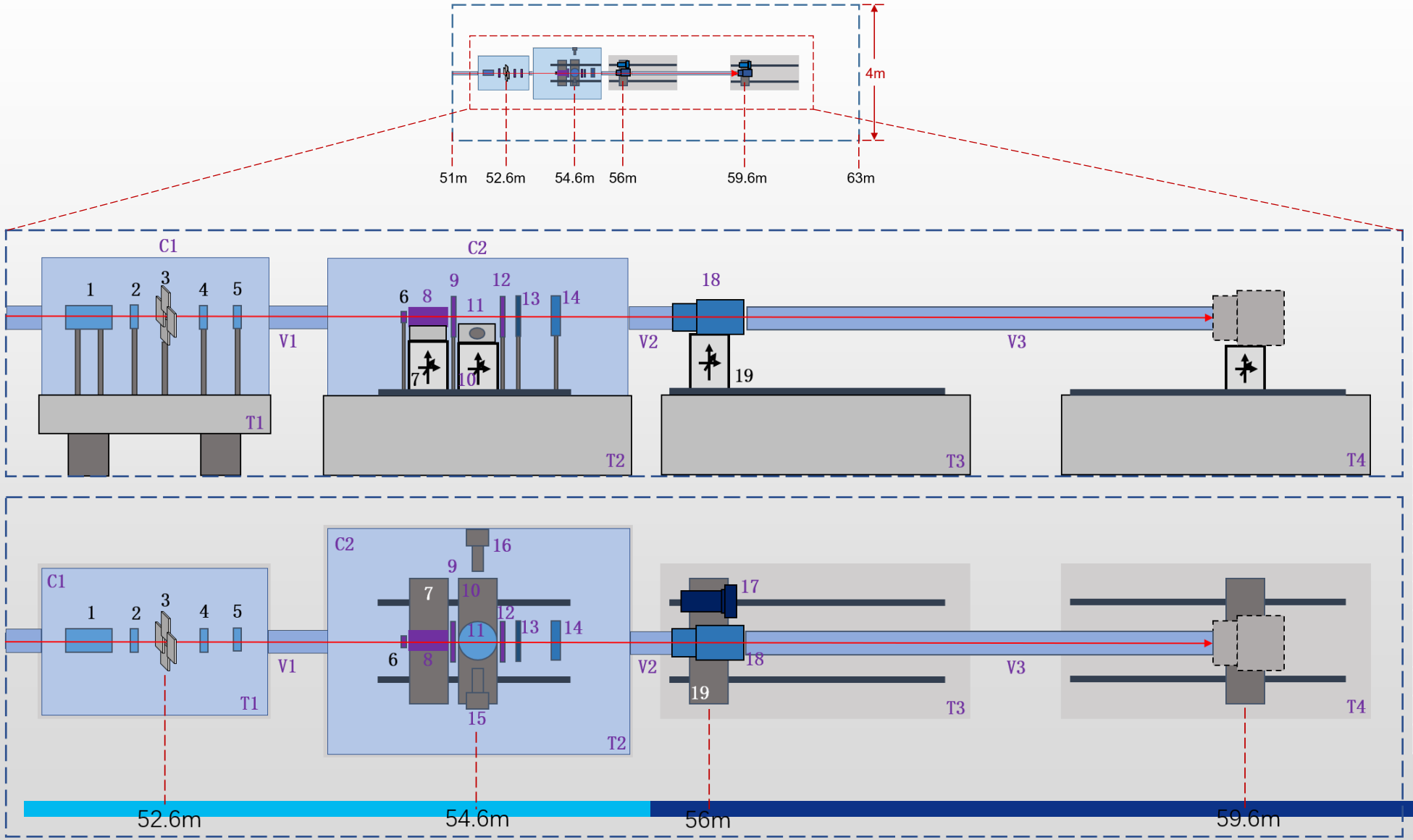


Shorten exposure time, fast nano-CT imaging

TXM beam-SILF

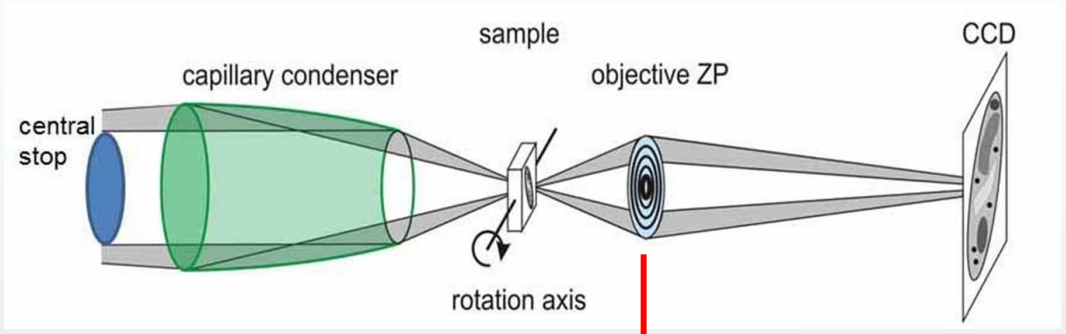


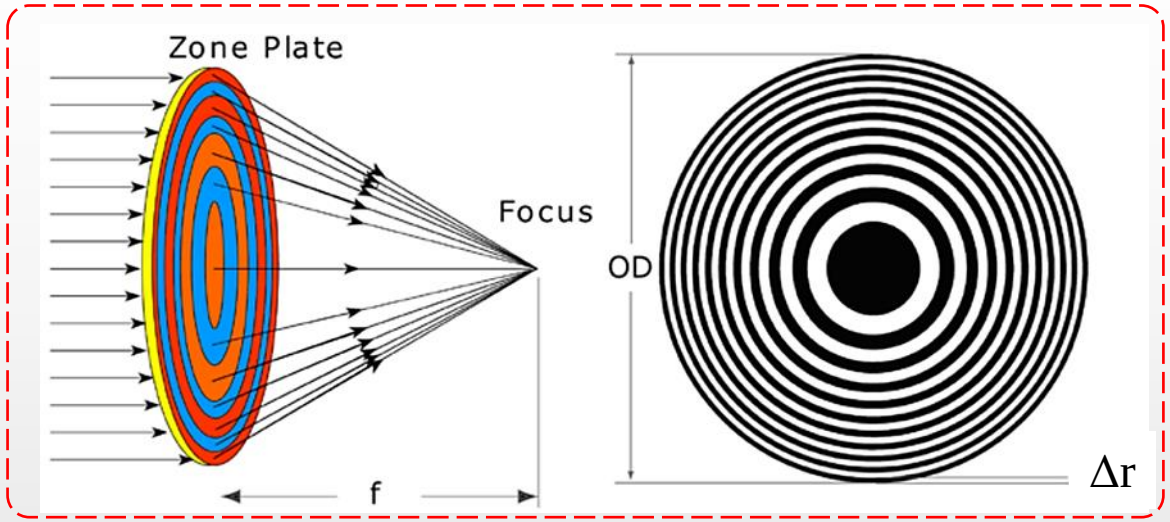
Layout



No.	Apparatus
1	Attenuator
2	Bpm
3	Slits
4	Diffuser
5	Ion chamber
6	Beamstop
7	Adjustment stage for elliptical focusing mirror
8	Elliptical focusing mirror
9	Pinhole
10	Sample stage
11	Rotary stage
12	Zone plate
13	Phase ring
14	Bertrand lens
15	Optical microscope
16	Telescope
17	Low-spatial-resolution detector
18	High-spatial-resolution detector
19	Multi-dimensional adjustment stage
T1-t4	Optical table
C1-c2	Polycarbonate chamber
V1-v3	Vacuum corrugated tube

Key device of TXM: zone plate





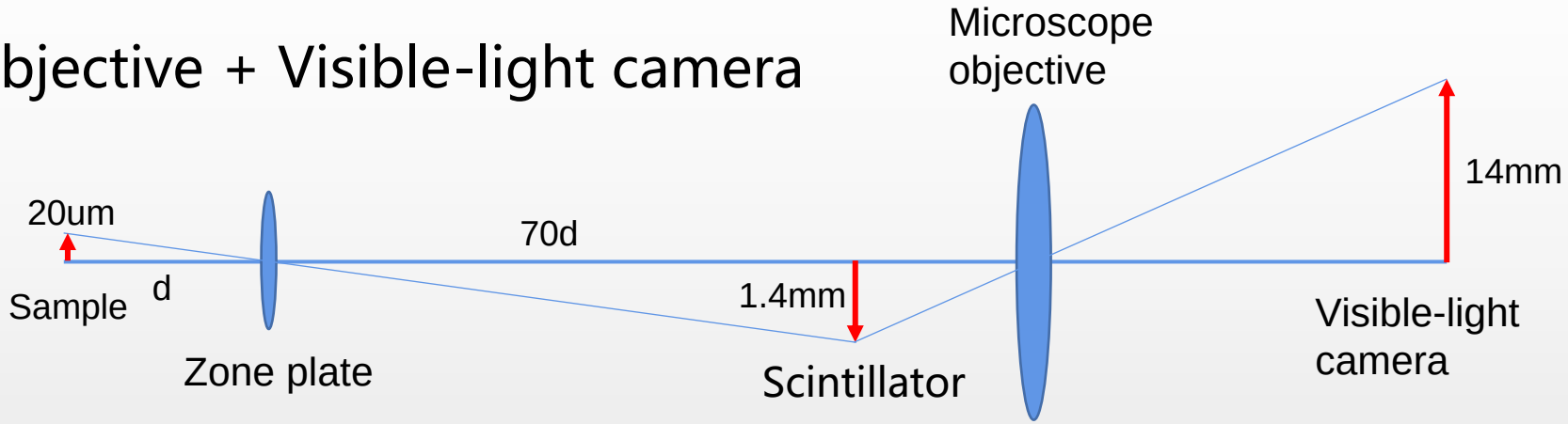
The spatial resolution δ depends on the outermost width Δr of the zone plate, with the relationship $\delta = 1.22\Delta r$. Given the target spatial resolution of 30 nm, the required outermost width for the zone plate is

$$\Delta r = \frac{30}{1.22}\text{nm} = 24.59\ \text{nm}$$

This experiment endstation uses a zone plate with an outermost zone width of 24.59 nm. Similar to the lens in an optical microscope, the lateral magnification of the zone plate is the ratio of the image distance to the object distance.

Distance between the zone plate and the detector

Scintillator + Microscope objective + Visible-light camera



Assuming a pixel pitch of 7 μm and 2000(H)×2000 (V) resolution for the camera, then the vertical size of the image plane is 14 mm. With a 10× microscope objective, the imaging size on the scintillator is 1.4 mm.

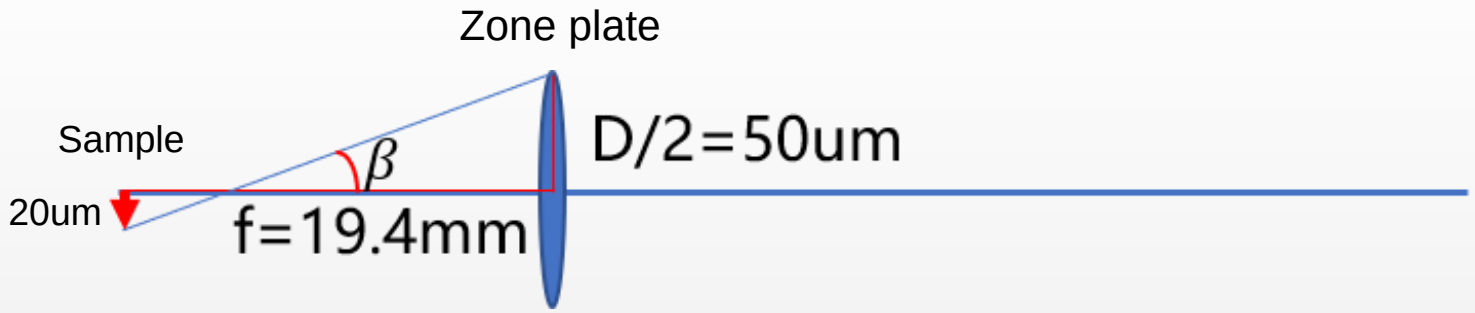
$$\frac{1}{d}+\frac{1}{70d}=\frac{1}{f}$$

$$d \approx 20\ \mathrm{mm}$$

$$70d \approx 1.4\ \mathrm{m}$$

Therefore, at least 1.4 m is required between zone plate and camera.

Phase space at the sample position



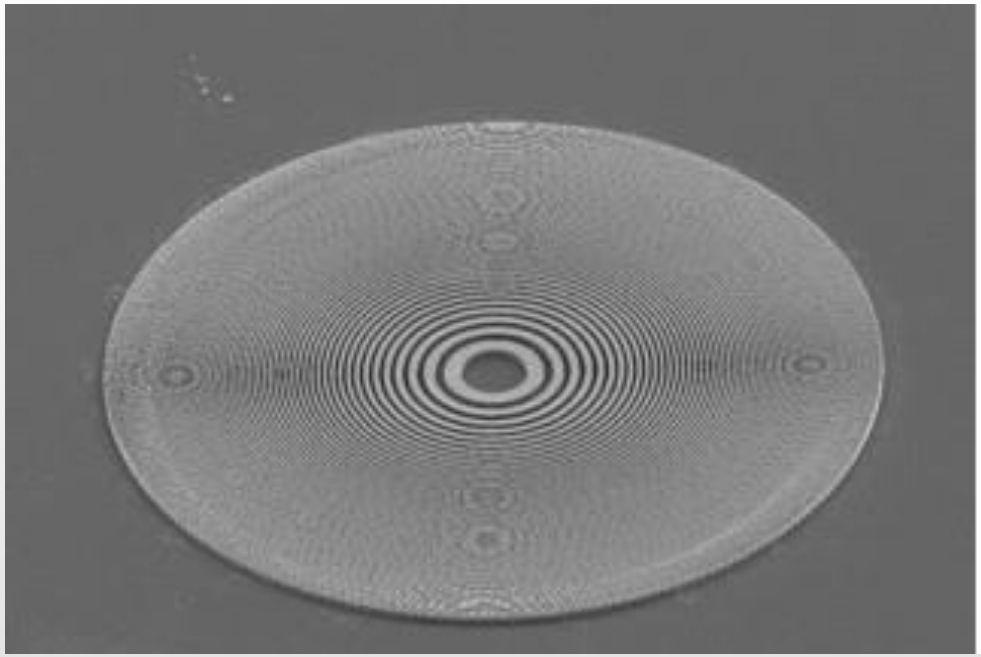
As shown in the figure above, given a focal length $f = 19.4\ mm$ and a zone plate diameter $D = 100\ \mu m$,

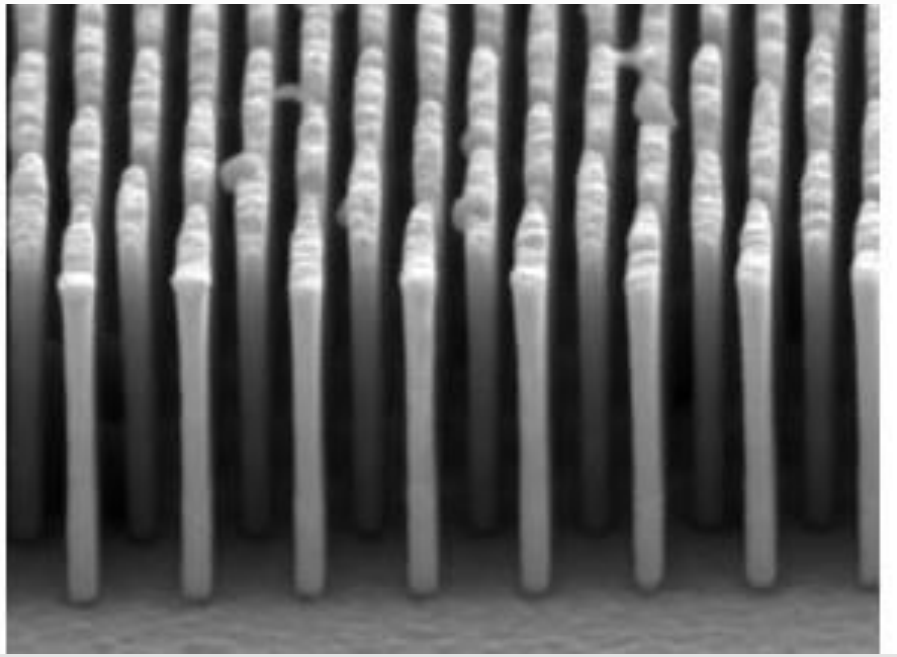
$$\tan\beta = \frac{D/2}{f} = \frac{100/2\ \mu m}{19.4mm} \approx 2.5 \times 10^{-3}$$

$$\beta \approx 2.5\ mrad$$

Therefore, divergence angle of incident beam should be $2\beta = 5\ mrad$, with a selected field of view (FOV) of $20\ \mu m$, the required illumination beam phase space at the sample position should be $100\ \mu m{-}mrad$.

Zone plate parameters



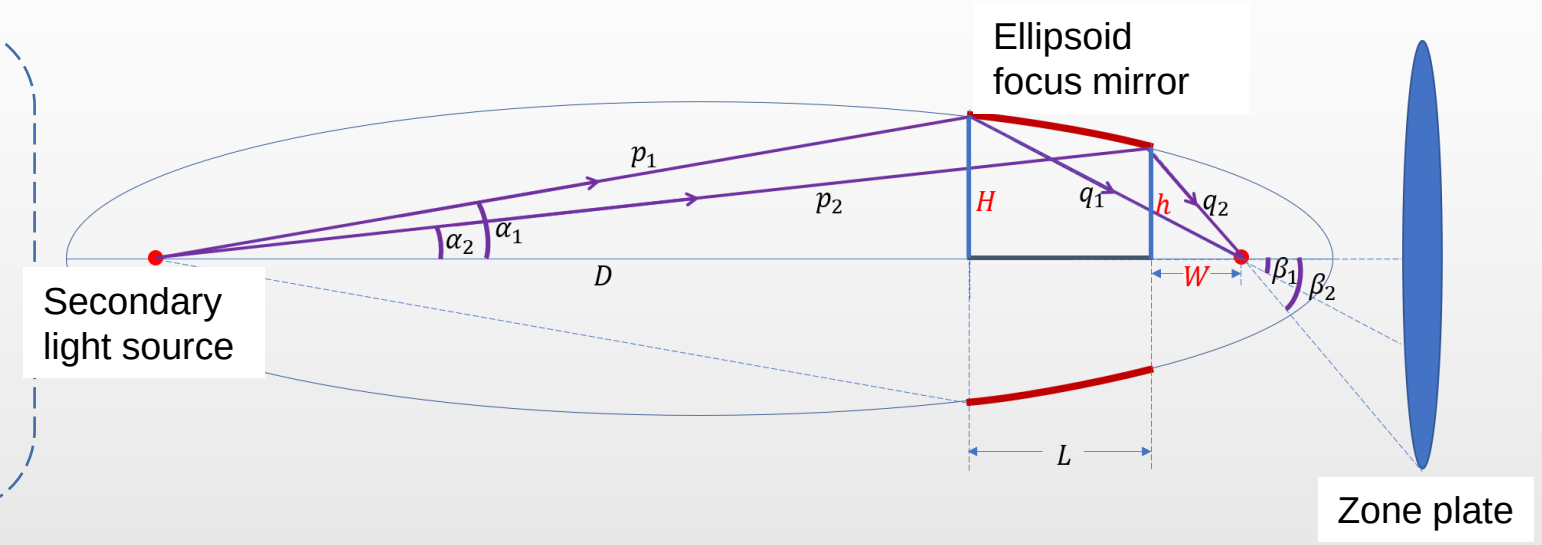


Energy /keV	Outermost Zone Width Δr /nm	Diameter D/μm	Focal length f/mm	Sample-detector distance/mm	Field of view /μm	Resolution /nm
5~11	24.59	100	19.4	700-1500	20	30
5~11	24.59	200	38.8	700-1500	40	50

Ellipsoid focus mirror

$$\tan\beta = \frac{D/2}{f} = \frac{100/2\,\mu m}{19.4mm} \approx 2.5 \times 10^{-3}$$
$$\beta \approx 2.5mrad$$

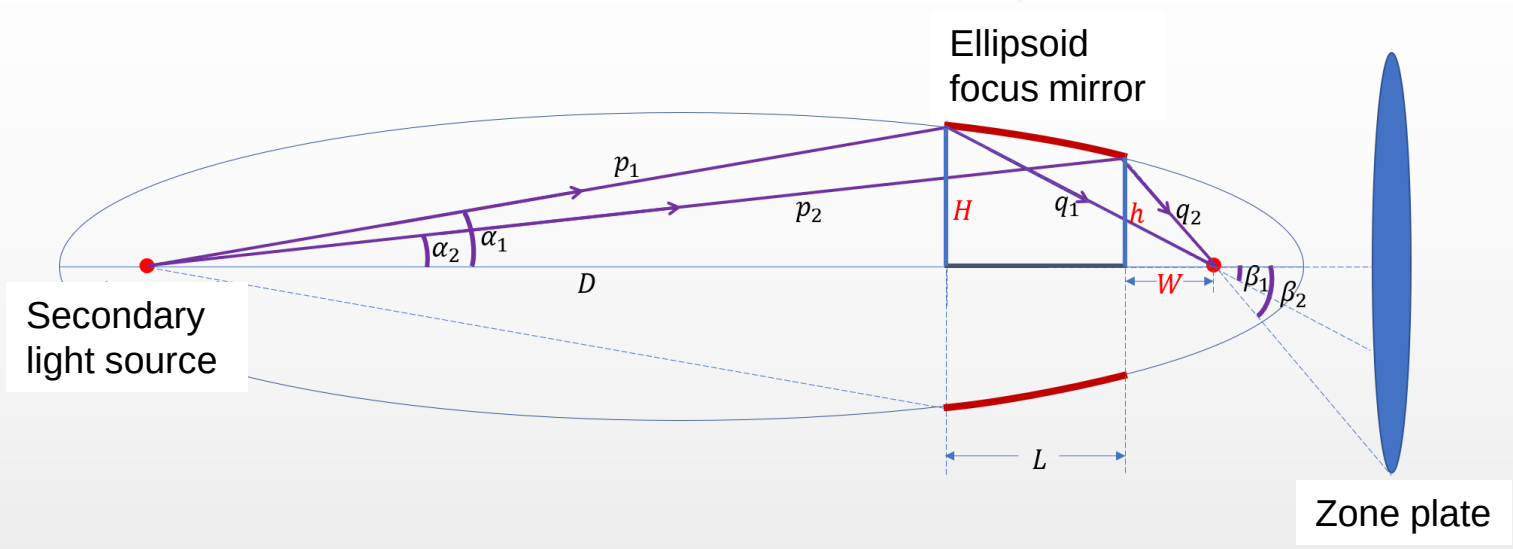
$$p_1 + q_1 = 2a$$
$$p_1 \sin\alpha_1 - q_1 \sin\beta_1 = 0$$
$$p_1 \cos\alpha_1 + q_1 \cos\beta_1 = 2c$$
$$b^2 + c^2 = a^2$$



Where a is the semi-major axis of the ellipsoid, b is the semi-minor axis, c is the semi-focal length, α_1 is the acceptance angle of the ellipsoid mirror, $\beta_1$and β_2 are the angles between the reflected light and the major axis of the ellipsoidal mirror. Due to the high eccentricity of the ellipsoidal focusing mirror, L is used to represent the arc length, i.e., the length of the ellipsoidal mirror $\approx L$.

Ellipsoid focus mirror

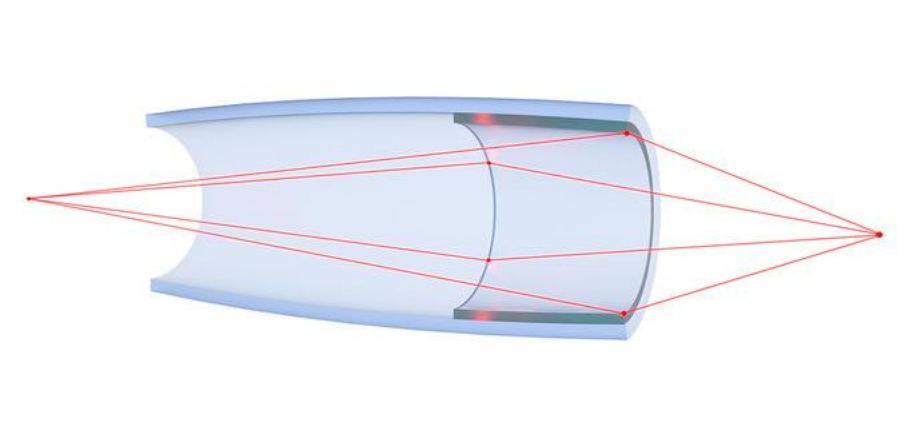
$$L = q_1\cos\beta_1 - q_2\cos\beta_2$$
$$W = q_2\cos\beta_2$$
$$H = q_1\sin\beta_1$$
$$h = q_2\sin\beta_2$$



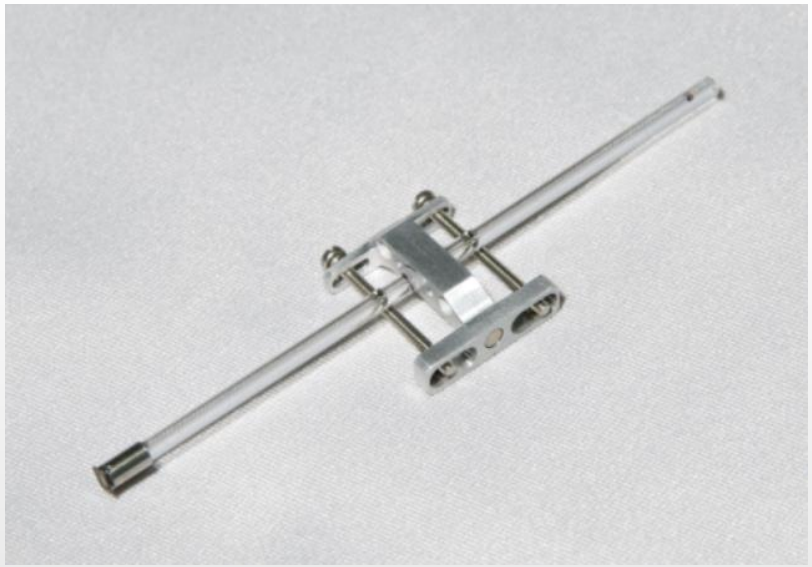
Where W is the working distance, H is the entrance radius, and h is the exit radius. TXM requires that the numerical aperture of the ellipsoidal focusing mirror should match that of the zone plate, which is $\beta_2 \approx \beta$ with $\beta = 2.5\,mrad$. Selecting the distance from the secondary light source to the ellipsoid focusing mirror as $1900\,mm$, $W = 46\,mm$, $L = 100\,mm$, $H = 0.195\,mm$, and $h = 0.115\,mm$. Then the half acceptance angle can be calculated through cosine law as $\alpha_1 = 103\,\mu rad$.

Therefore, the end station requires the divergence angle of the beam from the secondary light source $\geq 2\alpha_1$, which is $206\,\mu rad$.

Ellipsoid focus mirror parameter



Schematic of ellipsoid focus mirror



Real photo of ellipsoid focus mirror

Energy /keV	Half acceptance angle δ /mrad	Half emission angle σ /mrad	Distance from the secondary light source to the ellipsoid focus mirror p /mm	Distance from the ellipsoid focus mirror to sample point q /mm
8	0.103	2.5	1900	46

Members



Prof. Lei Li



Dr. Yan Zhang



Mr. Zengguang Tang



Dr. Xiaosheng Lin





湾区之光，由你点亮！

Join us, brighten the bay, smart the world



IASF 深圳综合粒子设施研究院
Institute of Advanced Science Facilities, Shenzhen

深圳市光明区圳园路268号
美华美工业区A3栋

Building A3, No. 268 Zhenyuan St, Guangming District,
Shenzhen, Guangdong, P.R.China